Advanced Aerodynamic Applications with the elsA Software

J. Reneaux, P. Beaumier, P. Girodroux-Lavigne

J. Reneaux, P. Beaumier, P. Girodroux-Lavigne
(Onera)

E-mail: joel.reneaux@onera.fr

Advanced Aerodynamic Applications with the *elsA* Software

Numerical simulation capability is one key differentiating factor in designing efficient transportation systems. With advanced numerical simulation capabilities, complex phenomena involved can be taken into account. This is illustrated in this paper through several research studies. All the simulations were carried out with the *elsA* software developed at Onera.

In terms of performance prediction, the capabilities of the CFD software are highlighted with various applications related to aircraft drag, control surface efficiency, high-lift configuration performance and store separation. Unsteady simulations are carried out to investigate complex interactions and off-design conditions: jet simulation, buffet prediction and dynamic stall. The importance of the coupling of different disciplines is underlined through aeroelastic, aero-acoustic and aero-thermal applications related to aircraft, helicopter rotors, engine compressors and turbines.

Performance improvement for transportation vehicles can be studied with optimization and flow control techniques. The adjoint approach has been used to optimize pylons and winglets for transport aircraft and helicopter rotor blades. Flow control is regarded as a key evolution offering new solutions for performance improvement. Control of buffet onset with Vortex Generators and separation control with synthetic jets for helicopter fuselages is presented to highlight the *elsA* software's ability to simulate actuator effects.

Various innovative concepts have been investigated using the *elsA* software. The flying wing, the supersonic business jet, the UCAV configuration, the Counter Rotating Open Rotor and the Tilt Rotor configurations are among the most promising ones.

Introduction

CFD capabilities are now widely used in the aerodynamic process of any transportation system. In particular, the design and the optimization of any aerodynamic shapes are based on intensive CFD applications. The CFD approach is also more and more frequently used for the determination of aerodynamic data for performance, loads and handling qualities.

The drag component can usually be determined in cruise conditions by the use of the Reynolds Averaged Navier-Stokes equations. On the other hand, off-design conditions and complex interactions sometimes require an unsteady approach such as the RANS/LES Simulation method. In order to improve the performance of the vehicle, the design problems can be tackled with Multi-Disciplinary Optimization. Flow control technologies are also promising for enhancing the aerodynamic behavior of the configuration. Aeroelastic and aero-acoustics issues will play a greater role in modern aerospace vehicles. To address all of these issues, Onera has been developing the *elsA* software [1], which deals with internal and external aerodynamics from the low subsonic to the high supersonic flow regime. A large variety of turbulence models from eddy viscosity to full Differential Reynolds Stress Models are implemented in *elsA* for the Reynolds Averaged Navier-Stokes approach. High flexibility advanced techniques involving multi-block structured meshes are available in *elsA* for handling complex configurations: these techniques include patched grid and overset capabilities (Chimera technique). The flow equations are solved by a cell-centered, finite-volume method. Space discretization schemes include second order upwind or centered schemes. The semi-discrete equations are integrated using a backward Euler approach with implicit schemes solved by robust LU relaxation methods. The convergence is improved by the use of multi-grid techniques for steady flows.

The numerical simulations must be assessed against detailed databases for all the configurations studied and for the various flow characteristics. For each specific application, Onera carries out research projects to establish broad and accurate experimental databases including advanced measurements:

- Static and unsteady pressure acquisitions through pressure taps and pressure transducers;
- Velocity measurements in the field using PIV and LDV techniques;
- Measurement of model surface deformation with strain gauges or optical methods.

For example, the availability of field measurements makes the development and the assessment of the turbulence models and the RANS/LES approach much easier.

The various applications presented in the following sections underscore the capabilities of the *elsA* software to simulate the flow physics that is involved in non-linear effects and in complex interactions. As the *elsA* software is currently used by many aircraft, helicopter, missile and engine makers, the examples are taken from this wide variety of applications.

Performance prediction

Aircraft drag prediction

In order to enhance its knowledge of the capabilities of CFD software to evaluate the drag of transport aircraft, the Onera Applied Aerodynamics Department participated in the 4th AIAA Drag Prediction Workshop held in San Antonio, Texas in June 2009 [2]. The focus of the DPW4 was on drag and moment prediction accuracy for the new wing/body/horizontal-tail NASA CRM (Common Research Model) configuration. This workshop included a grid convergence study (multi-block structured grids from 5.10^6 nodes to 50.10^6 nodes provided by Boeing) and a downwash study (lift polars with tail-off and tail-on at 3 deflection angles). The aerodynamic conditions were the following: Mach=0.85 (design point) and Re=5.10^6 (NASA Ames 11-ft transonic wind tunnel conditions). Experimental data for the CRM is expected to be available in 2010; it will be used for comparison and validation purposes. The *elsA* calculations were carried out with the Spalart-Allmaras turbulence model in fully turbulent conditions. The solutions were finally post-processed with the Onera ffd72 far-field drag extraction tool [3].

Figure 1 presents the results from *elsA* simulations (contours of pressure) on the NASA CRM configuration including the horizontal tail plane. Figure 2 shows the viscous and wave drag integration volumes used by the ffd72 software. It is necessary to obtain a physical drag breakdown and therefore to eliminate artificial drag. This capacity is very helpful for aircraft makers. For instance, it can be seen here that no wave drag is produced on the tail.

Very good agreement has been observed between the Onera-*elsA* results [2] and the near-field drag coefficients (pressure and friction) computed by other DPW4 participants such as Airbus, Boeing and DLR (less than 2 drag counts of difference over around 275 of total drag counts for the structured mesh approach, a drag count being 10^{-4}). Furthermore, the far-field drag extraction tool ffd72 has given Onera the singular capability of presenting the values of the different physical drag components. For example, at M=0.85 and C_L=0.5, the different drag components of the configuration under consideration expressed as a percentage of the total drag are the following: viscous drag 64% (friction drag 47% plus viscous pressure drag 17%), lift-induced drag 34% and wave drag 2%.

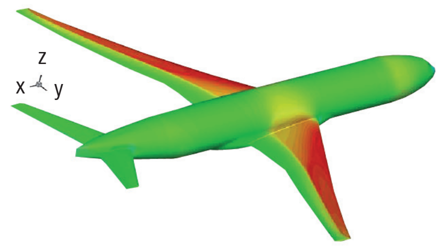

Figure 1 – RANS computation on the NASA CRM configuration of the 4th AIAA Drag Prediction Workshop

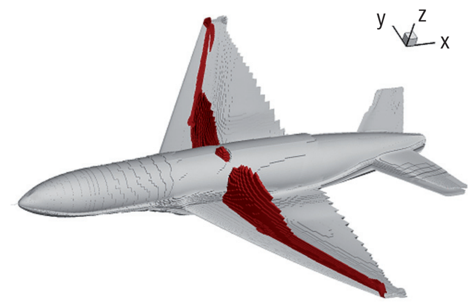

Figure 2 – Far-field drag extraction on the NASA CRM – Viscous drag (grey) and wave drag (red) productions

Control surfaces

The determination of the efficiency of control surfaces is an important topic for the design of a modern aircraft and this must be done early in the design process. The *elsA* software and the overset technique allow for dissociation of the structured topologies of various elements. The mesh quality of each component is increased, but complexity arises

Box 1 - Far field drag extraction

The far-field drag extraction techniques [3] which have been developed by Onera over the past years, allow the spurious drag to be identified and removed from the drag breakdown. This spurious drag component depends on the grid refinement and quality, on the amount of artificial dissipation introduced by the numerical scheme, and on the aerodynamic conditions.

In addition, far-field drag extraction is able to produce a physical drag breakdown, which is more useful to the aerodynamicist than the pressure plus friction breakdown. This is based on the distinction between irreversible and reversible thermodynamic processes. The former imply a change in energy form and are responsible for viscous drag and wave drag. The latter involve only exchanges of mechanical energy and are responsible for induced drag. An additional advantage of the Onera drag extraction method is the possibility of obtaining a spatial distribution of the local drag.

A designer using far-field extraction besides the simpler near-field integration is then in a position to produce a more efficient shape in a smaller number of redesigns.

in the assembly phase of the various meshes. This is why Onera launched a project devoted to improving the overset technique and its assessment with a detailed experimental database [4].

The model represents a large civil transport aircraft equipped with spoilers and ailerons. The test was carried out in the Onera S2MA wind tunnel with detailed measurements such as a six-component balance, hinge moment balances for spoilers, steady and unsteady measurements, and wake surveys.

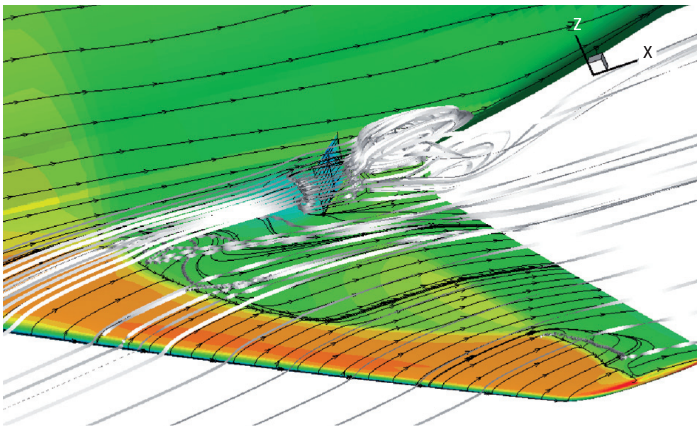

Figure 3 – RANS simulation around a spoiler in transonic flow, M=0.85, δ=45°, α=3°

An example of a computation with the Spalart Allmaras turbulence model is presented in figure 3 for the configuration equipped with a 45° spoiler at M=0.85. The visualization underscores the complexity of the flow with strong separations upstream and downstream of the spoiler and with a deviation of the shock position compared with the span.

A comparison with the experimental results is presented in figure 4 considering pressure measurements at mid-span of the spoiler (y/b=0.255). We can see that the CFD results agree rather well with the measurements with a good level of the computed pressure downstream of the spoiler. Many comparisons, such as the one presented above, have demonstrated the capability of the overset mesh technique to accurately predict the efficiency of the control surfaces.

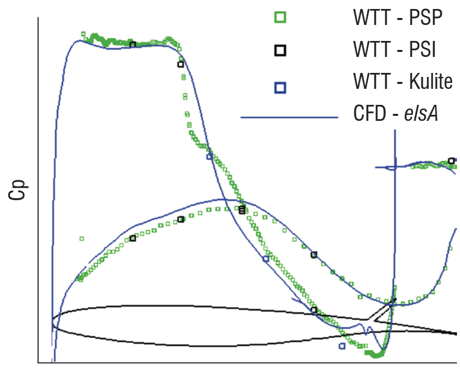

Figure 4 – Comparison between *elsA* simulation and experiment at mid span of the spoiler, M=0.85, δ=45°, α=3.95°

High-lift configuration

Aircraft performance prediction in high-lift configurations requires good modeling of several complex phenomena such as separation and wake/boundary layer interactions, local compressible flow embedded into dominantly incompressible low Mach number regions and the transition from laminar to turbulent flows on each element. Among the various topics, an accurate estimation of the maximum lift coefficient early in the design stage is of prime importance for designers. Consequently, the following different transition mechanisms must be considered in the CFD process: Tollmien-Schlichting (TS) and cross-flow instability growths, attachment line contamination (ALT), relaminarization and separation bubble.

Transition prediction capability has been introduced into the *elsA* code, based on the application of criteria that were developed at Onera for use in boundary layer codes. A recent implementation of a new method [5] led to the elimination of most of the topology limitations. For the streamwise instability mode, the TS criterion or the e^N method combined with Mack's relationship can be considered in combination with the Gleyzes-Habiballah criterion for 2D short bubble transition. It allows for prediction of the transition location depending on the freestream turbulence level. Crossflow instability modes have also been taken into account with a criterion based on the displacement thickness in the crossflow direction. An intermittency function γ is used to simulate the transition region.

In the framework of the Eurolift II project, several configurations have been considered for validation purposes [6]: a clean wing configuration at low speed, a generic high-lift rectangular wing and a more realistic three-dimensional high-lift configuration with a full span slat and flap (figure 5).

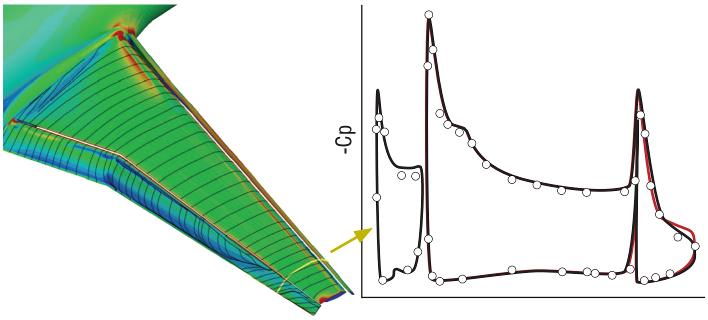

Figure 5 – Eurolift 2 configuration. $M=0.178$, $Re_c=1.38\times10^6$, $\alpha=10^o$ Symbols: experiment, Red: fully turbulent computations, Black: transition computed internally

With a 5.5 10^6 node grid provided by Airbus-Deutschland and the Spalart Allmaras turbulence model, the turbulent RANS simulation matches the experiment (Airbus-D LSWT wind tunnel test) rather well on the various elements of the wing with a slight deviation near the tip. Taking transition into account, the agreement on the flap is much better as observed on the right side of figure 5 with the disappearance of the local flow separation on the upper surface of the flap.

The use of transition prediction methods in the *elsA* software has significantly improved the performance determination for such complex configurations. Moreover, the overset grid capability offered by the *elsA* software is also an asset in dealing with the detailed 3D geometries of the actual high-lift configurations.

Jet simulation

The diameter of the engines of transport aircraft has been regularly increased in recent years, requiring that they be placed nearer the wing because of ground clearance and structure constraints, thus leading to a strong interaction between the jet and the pylon. To investigate the RANS and ZDES capabilities for predicting these interaction phenomena, advanced simulations were carried out on a power-plant configuration for which a large database was assembled in the Onera S3Ch wind tunnel of the Fundamental and Experimental Aerodynamics Department (DAFE) [7].

The wall-to-wall wing model equipped with pylon and nacelle was installed in the 0.8 x 0.8 m^2 S3Ch test section of the Onera Meudon Center. The nacelle was studied and manufactured to simulate both the engine fan and core jets using an air supply system installed upstream of the nacelle. Care was taken to limit the influence of the boundary layer which develops on this system, considering boundary layer suction. The pressure ratios of the jets can be varied during the tests and the core jet temperature can be slightly increased to investigate the thermal effects. Upper and lower walls were defined to limit wall interference effects. An accurate database was established using up-to-date measurements. Probes and laser (LDV, PIV) measurements were used and analyzed considering averaged and RMS values of the flow velocity.

Simulations were carried out using the broad and accurate experimental database. These simulations were performed in order to match experiments as much as possible and for thorough assessment, including the turbulent field in the jet. Two different structured grids of respectively 20 and 40 million nodes were defined to perform the simulations: mesh adaptations were carried out to capture the mixing layers in the jets. The patched grid technique was also used to reduce the size of the meshes. In the simulations carried out with the *elsA* software, fan and core jets were introduced thanks to injection type boundary conditions. Hybrid RANS/LES methods have attracted great interest over the past ten years as they combine the best features of the Reynolds Averaged Navier-Stokes and of Large Eddy Simulations. A Zonal DES approach [8] was chosen to avoid any difficulties when switching from the RANS to the LES mode. In this approach, the grid refinements can then be applied to the regions of interest, avoiding any detrimental influence on the boundary layer properties.

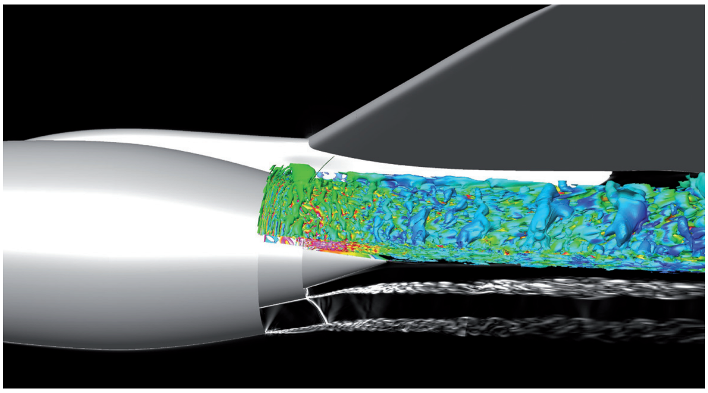

Figure 6 – Q-criterion and Schlieren type flow visualizations with Z-DES 40 10^6 nodes, $M=0.84$, $Re=6\ 10^6$

Figure 6 presents the DES results with both the Q-criterion and Schlieren type visualization. The rolling-up of eddies in the early stage of the fan jet mixing layer can be seen. Further downstream, these eddies become streamwise due to the entrainment effects. The mixing layers between the fan and the core jets as well as between the fan jet and the flow outside of the jet are well displayed.

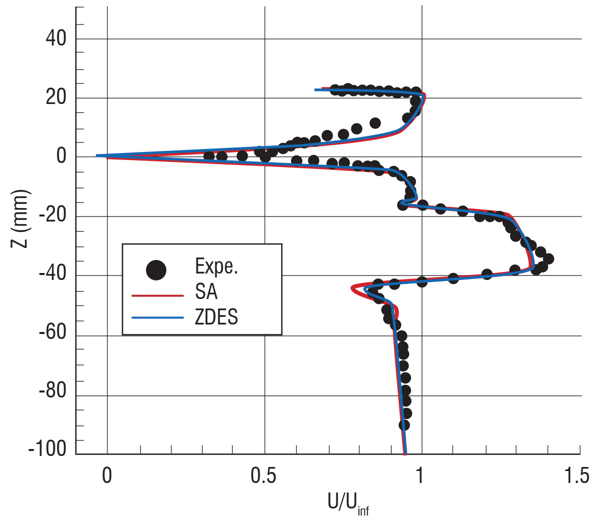

Figure 7 – Streamwise velocity profiles just downstream of the plug – Computation and S3Ch experiment

Box 2 - DES simulation

As emphasized in the introduction, new industrial needs in aerodynamics involve for example the control of noise as well as the ability to predict dynamic loads so that the simulation of 3D unsteady turbulent flows is required. It is now commonly accepted that hybrid RANS-LES is the best strategy to drastically reduce computation costs (compared to LES) in a wide range of complex industrial applications if attached boundary layers have a significant impact on the global flow dynamics.

However, two weaknesses in the use of hybrid methods for technical flows are classically identified (see [9] for a review). The first one concerns a possible delay in the formation of instabilities in mixing layers due to the advection of the upstream RANS eddy viscosity. The second one deals with the treatment of the “grey-area”, where the model switches from RANS to LES, and where the velocity fluctuations, the “LES-content”, are expected to be not sufficiently developed to compensate for the loss of modeled turbulent stresses. This can lead to unphysical outcomes, such as an underestimation of the skin friction and at worst may it can cause premature separation or “Grid-Induced Separation” (GIS).

In order to get rid of this latter drawback, Spalart et al.[10] proposed a modification of the model length scale presented as a Delayed Detached Eddy Simulation (DDES) to delay the switch into the LES mode to prevent “model-stress depletion” (MSD). In a different spirit, Deck [8][11] proposed a Zonal Detached Eddy Simulation (ZDES) approach, in which the RANS and DES domains are selected individually. The motivation is to avoid MSD and to clarify the role of each region. In practice, ZDES switches very quickly to the LES mode, thus limiting the grey area, which is responsible for the delay in the formation of instabilities. Moreover, the valuable aspect of this approach is that the user can focus his grid refinement on regions of interest without corrupting the boundary layer properties farther upstream or downstream.

The ability to simulate three-dimensional flows in the framework of applications (attached boundary layers treated in RANS mode) has already been demonstrated thanks to thorough comparison with the available experimental data including spectral and second-order analysis (see [12] for a review).

The computed mean velocity profiles are compared with experiments (LDV profiles) in the section just downstream of the plug in figure 7. Results obtained with ZDES and RANS simulations exhibit very close characteristics when averaged fields are considered. The mixing layers are very well predicted, the wake of the upper side of the plug is slightly underestimated. Some discrepancies could come from the system for injection into the nacelle which is not taken into account and simulated with uniform injection conditions.

The u’ w’ unsteady component is presented in figure 8 for the RANS and ZDES simulations, and the experiment at the location just downstream of the plug. This turbulent quantity is underestimated in the mixing layer between the fan jet and the outer flow by both simulations, especially the ZDES. The mixing layers between the core and fan jets are well predicted by the ZDES simulation and underestimated by the RANS approach. In addition, the ZDES method allows all the turbulent components to be computed easily, contrary to RANS simulation.

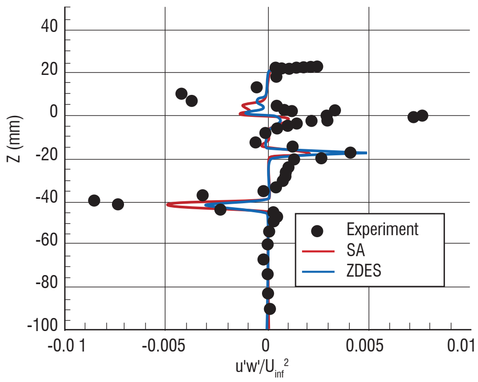

Figure 8 – The u'w' unsteady component just downstream of the plug - Computations and S3Ch experiment

The value of ZDES simulations for such configurations lies in the very large amount of information it produces together with direct access to the flow unsteadiness. This allows for a very deep analysis of turbulent structures inside mixing layers and of the interaction between the pylon wake and the jet. It is expected that the ZDES approach will open up new possibilities in the future for thermal effects and airframe noise prediction.

Simulation of phenomena at the limits of the flight domain

Buffet prediction

Aircraft in flight can be subject to buffet excitation. This phenomenon is defined as the structural response to an aerodynamic excitation produced by boundary layer separations. In the case of civil transport aircraft, buffeting may cause discomfort for passengers and difficulty for the pilot to control the aircraft and can also lead to structural fatigue. Thus, buffeting limits the flight envelope in terms of lift coefficient - Mach number boundaries. The buffet onset is measured in wind tunnels using models equipped with accelerometers and unsteady pressure transducers. The prediction of buffeting in flight remains difficult however. From the aerodynamics side, the scale effects modify the extent of flow separation areas. Moreover, wind tunnel models do not have scaled inertial properties.

This is why a combined experimental and numerical approach is important to better understand and predict the physical phenomena linked to the fluctuating pressures. Hence, the Detached-Eddy-Simulation could be used to predict the main instabilities of the flow and to improve the extrapolation of wind tunnel results to flight conditions.

The assessment of the DES approach was carried out considering a wing body configuration which was tested in the S3Ch transonic research wind tunnel of the Onera Meudon center. The patched-grid method is applied in order to perform accurate simulations in the ZDES region and to limit the grid density in other RANS regions. The grid is composed of about 33 million nodes, most of them in the ZDES separated region. A simulation was performed at M=0.82, Re = 3 10^6, in established buffet conditions.

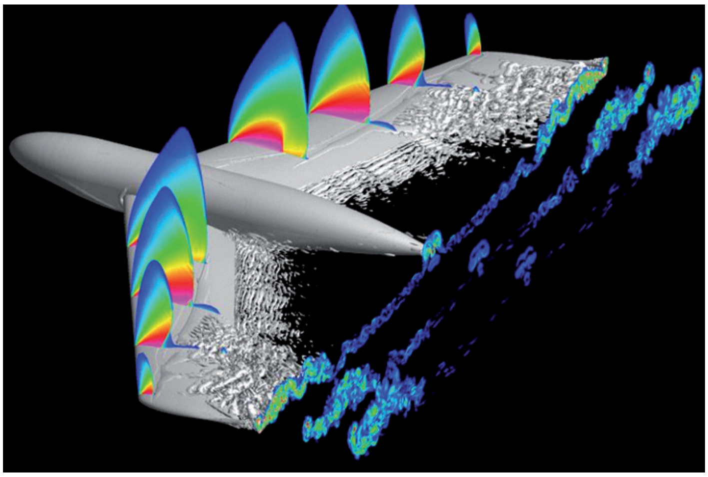

Figure 9 – ZDES computation in buffet condition. M=0.82, α=3.5°

In these flow conditions, a massive separation occurs and extends from the shock foot to the trailing edge in the outer part of the wing. This separated area is highly unstable and triggers the shock movement, and the buffet. The Q-criterion in figure 9 shows the roll-up of eddies in the separated area and the effect of the instabilities of the separation and the shock shape. This phenomenon, characterized by a moving separation line as well as a separation located close to the upper surface of the wing, is a very challenging and complex test case for a DES-type simulation.

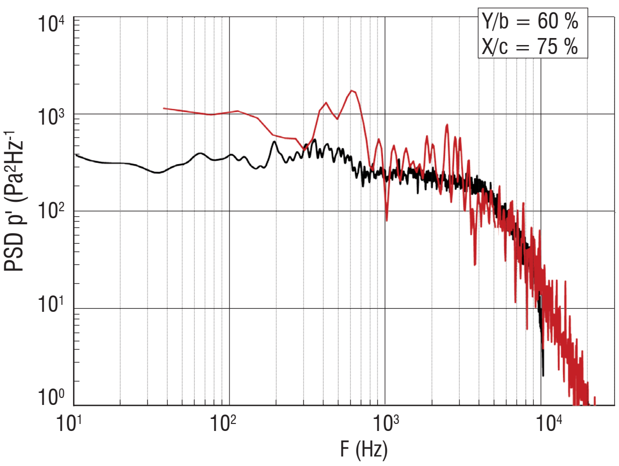

Figure 10 – Comparison of power spectral density in ZDES simulation and experiment

The power spectral density of the fluctuating part of the pressure signal at the upper side of the wing inside the separation is compared in figure 10 between an experiment and the ZDES simulation. It appears clearly that levels in the low frequency band are slightly overestimated but are properly predicted in the higher frequencies. Indeed, in these flow conditions, the buffet phenomenon is slightly over estimated which is probably the consequence of a still too coarse grid in the separated region. Nonetheless, only ZDES type simulations allow such spectra to be obtained.

Dynamic stall

Among aerodynamic issues encountered on helicopter rotors, dynamic stall [13] is certainly the most challenging, both in the understanding of the physical phenomena and their numerical simulation. Dynamic stall mainly occurs on the retreating blade side, where the blade operates under small velocities and large angles of attack. In these conditions, the flow over the blade section separates abruptly with the formation of a strong dynamic stall vortex that leads to a brief increase of maximum lift and very large negative pitching moments, with consequences on the aeroelastic stability of the rotor.

The numerical prediction of such unsteady, turbulent, compressible flows is very complex. Several Onera internal projects have been dedicated to this topic. In the PRF "Dynamic Stall", large efforts were made in order to get rid of numerical errors as much as possible by trying to define well-adapted refined grids. From a modeling standpoint, the sensitivity of the numerical results to the modeling of turbulence has been assessed and one of the main conclusion is that it is essential to be able to capture the laminar to turbulent boundary layer transition as accurately as possible in order to obtain results not too far from the measurements, at least when the Mach number is low (M< 0.2).

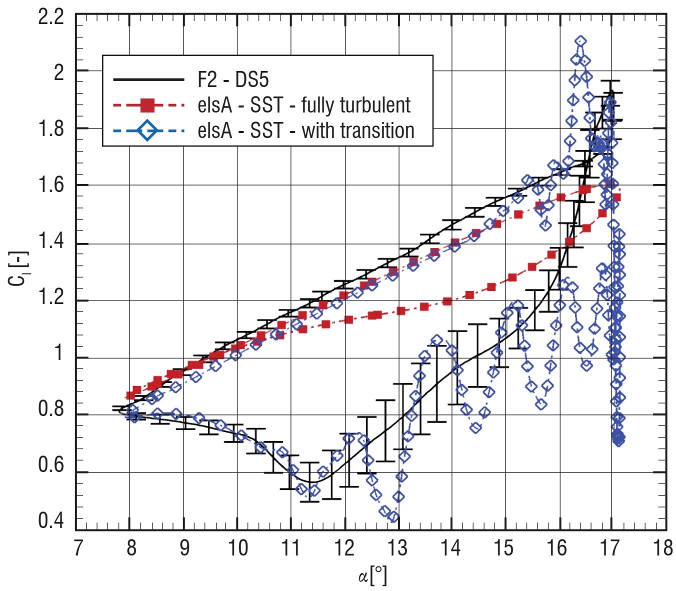

Figure 11 – Cl history of the OA209 airfoil under dynamic stall. α=12.5°+/-4.6°, k=0.1, Re=1.10⁶, M=0.1617

As an example, figure 11 shows the lift history of the OA209 airfoil under dynamic stall conditions: the fully turbulent calculation in red is unable to predict the large hysteresis effects present in the measurements. When an adequate transition model is applied (blue curve), the predicted lift history becomes much better compared to the experiment, even if the airfoil tends to stall slightly too early.

However, transition is not the only concern as shown by figure 12 where the iso-contours of the velocity field are compared with the F2 experiment at the beginning of the downstroke for 2 fully turbulent computations, one with the SST and the other with the EARSM model. While the first turbulence model does not provide any stall, but only very limited trailing edge separation, the algebraic Reynolds stress model does predict stall, although the leading edge separation is still missed.

Research efforts are now being oriented towards more advanced numerical models such as DES, LES or coupled RANS-LES methods in order to improve the fidelity of the numerical approach. The validation of these methods has been initiated for simple conditions (2D oscillating airfoil), but today would require computational efforts that are too large for realistic applications (3D rotating blade). Another important research orientation is the acquisition of experimental databases that are accurate enough not only to validate the calculations but also to improve our understanding of the physics. This is one of the objectives of the on-going Simcos project, which aims at developing technologies to control dynamic stall. Promising wind-tunnel test results were recently obtained through the use of deployable leading-edge vortex generators.

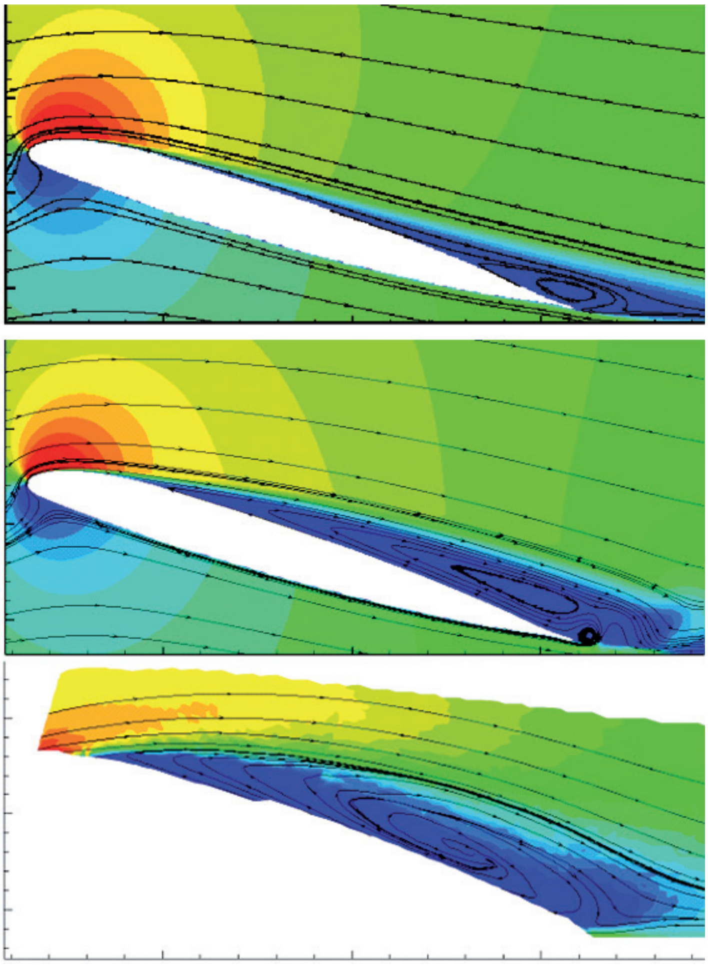

Figure 12 – Effect of turbulence model on the mean velocity around the OA209 airfoil under dynamic stall. Top: *elsA* (SST, fully turbulent). Middle: elsA (EARSM, fully turbulent). Bottom: LDV measurements. $\alpha=17°\downarrow$, k=0.1, $Re=1.10^6$, M=0.1617

Store separation

With the increasing number of weapons carried under combat aircraft, the study of store separation is becoming more and more challenging. Moreover, the proximity and multiplicity of stores coupled with wider transonic firing ranges (over Mach 0.9) induce important flow interactions between the released weapon and the aircraft. To ease the meshing and flow simulation of such complex configurations, we can use the Chimera method implemented in *elsA*, which enables a discretization of the flow equations in meshes composed of overset structured grids.

Within the framework of a national project, numerical simulations as well as experimental wind tunnel tests were carried out and helped to calibrate and validate the *elsA* Chimera method on heavy weapon separation configurations. Figure 13 illustrates the insertion of a generic cruise missile under the wing of a combat aircraft at a specific separation position. It also shows the ability of the Chimera method to capture the flow interaction between the wing and the missile, especially the transonic interaction shocks.

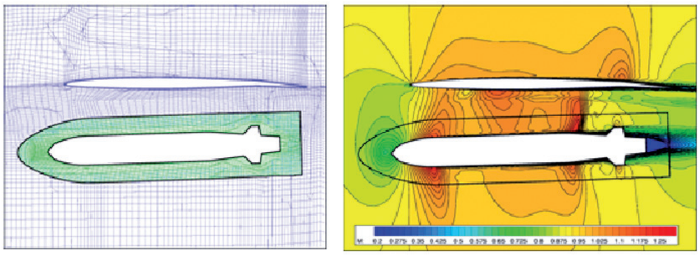

Figure 13 – Grid and Mach number in the symmetry plane of a generic cruise missile

The accurate simulation of a store separation requires the perfect restitution of the flow field under aircraft that are usually heavily loaded, which means meshing every carried store as finely as possible. Use of the Chimera method allows for separate accurate meshing of each store and its integration under the store free aircraft. This approach is used to analyze the aerodynamic characteristics of a rocket during its release from an aircraft. In this case, the tanks, the pod, the central pylon and the rocket are inserted in the grid of the plane limiting the number of nodes of the whole structured mesh to $15\ 10^6$ with a fine representation of each element.

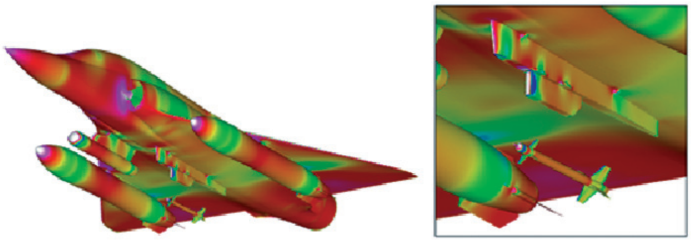

Figure 14 – Skin pressure in the case of the rocket separation

Figure 14 illustrates the skin pressure obtained in the early phase of the rocket separation. We can see the complexity of the flow field, especially around the pod and the pylon of the rocket. The Chimera technique allows for precise simulation of the complex flows under heavily loaded combat aircraft and for better prediction of the aerodynamic coefficients of the store while it is interacting with the carrier.

Within the framework of separation studies, another advantage of the Chimera method is that the released store can be repositioned anywhere under the aircraft without needing any mesh adaptation. This allows for quite simple CFD and 6 degrees of freedom flight mechanics coupling in order to compute the real trajectory of the store.

CFD - wind tunnel synergy

The CFD approach can also be used to better understand the flow quality in the wind tunnels and to improve the wall and sting correction methods [14], [15]. Simulations of the wind tunnel with the model and supports are facilitated by some characteristics of the *elsA* software such as the patched grid and overset capabilities.

One example is given in figure 15 with a set-up in a low speed wind tunnel. The model is installed on a mast and a survey device is used to carry out wake measurements. In this research, the RANS simulations have been used to investigate the interactions between the different elements and in particular their impacts on the drag component. The flow field distortion caused by the mast and the survey device were deduced by comparing simulations with and without supports.

From a more general point of view, simulations have demonstrated the need to carefully account for Mach number and angle of attack corrections for each support in order to achieve good accuracy.

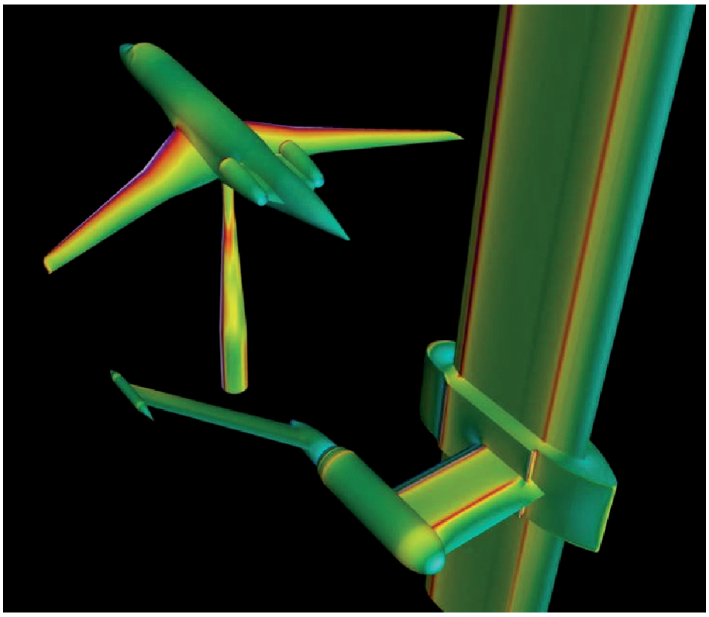

Figure 15 – Use of RANS approach to investigate the interactions between the model, the vertical strut and the probing devices in the F1 low speed wind tunnel

Aeroelasticity

Computational Aeroelasticity (CAE) is playing an increasing role in the design and analysis of aerospace vehicles. The two examples given in this section illustrate the current state of the CAE capabilities developed in the "Aeroelasticity and Structural Dynamics" Department for the two main areas of application: airframe and turbomachinery.

Static aeroelastic coupling on a transport aircraft

Accurate prediction of the steady state flow characteristics around a modern flexible transport aircraft requires the taking into account of structural deformations, through a fluid-structure static coupled simulation. This section demonstrates the static aeroelastic capability of the *elsA* software in the case of a wing/body/pylons/nacelles model [16] studied in the framework of the AWIATOR European project.

The multi-block structured grid used for the aerodynamic computation includes about 7 million nodes. A subset of structural nodes, located on the wing and winglet, has been selected in the Nastran finite element structural model, in order to build the reduced flexibility matrix which is used in the fluid-structure coupling process.

a)

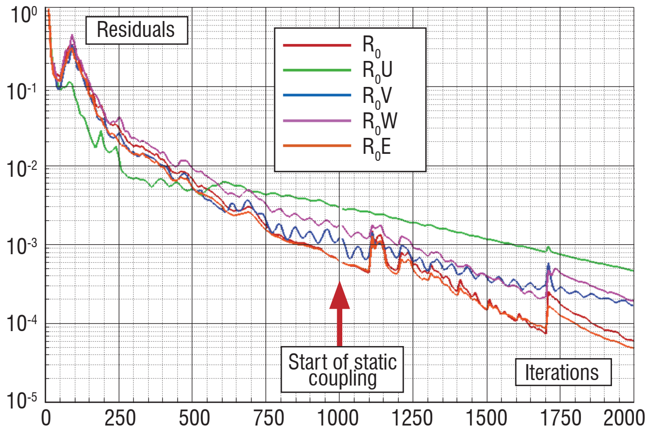

b)

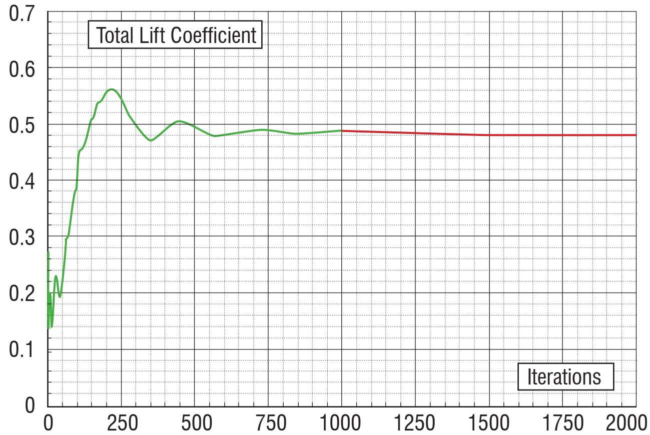

Figure 16 – Convergence of the mean flow residuals, and lift coefficient history

The flow conditions correspond to transonic speed at Mach number 0.82, for a flight altitude equal to 36,000 feet and a global lift coefficient equal to 0.49. The angle of attack has been adjusted in the numerical simulation in order to match this lift coefficient. Static coupling may be run in *elsA* starting either from the undeformed jig shape or from any deformed shape. In the latter case, it is necessary to provide the initial structural deformations. In the present case, the numerical simulation has been achieved starting from an initial "estimated flight shape" provided by Airbus.

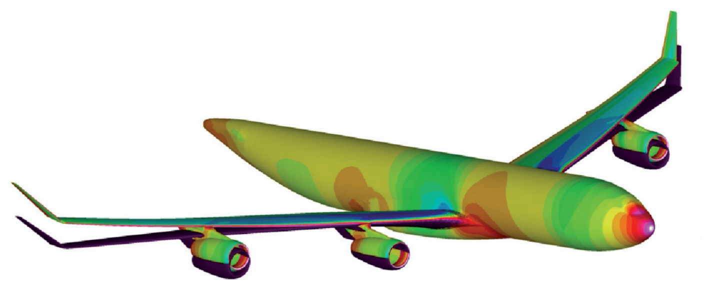

Figure 17 – Wall pressure on the AWIATOR configuration

The 1-equation Spalart-Allmaras turbulence model has been used for the turbulence modeling. 1,000 iterations were first performed without static coupling in order to get an aerodynamic field consistent with the initial estimated flight shape, and 10 coupling cycles, with 100 flow iterations per cycle, were then computed. The structural deformations and the aerodynamic grid are updated at each coupling cycle, using the mixed analytical Transfinite Interpolation mesh deformation technique included in *elsA*.

A 4-order magnitude decrease of the mean flow residuals was reached at the end of the simulation (figure 16). There was good agreement between the computed and measured pressure distributions in different wing sections, as shown in figure 17 and figure 18, although the computed shock locations are slightly more upstream in the middle region of the wing. As far as the wing deformations are concerned, it can be seen in figure 19 that the predicted spanwise wing vertical bending and twist deformations compare very well with the flight test measurements using the photogrammetry technique.

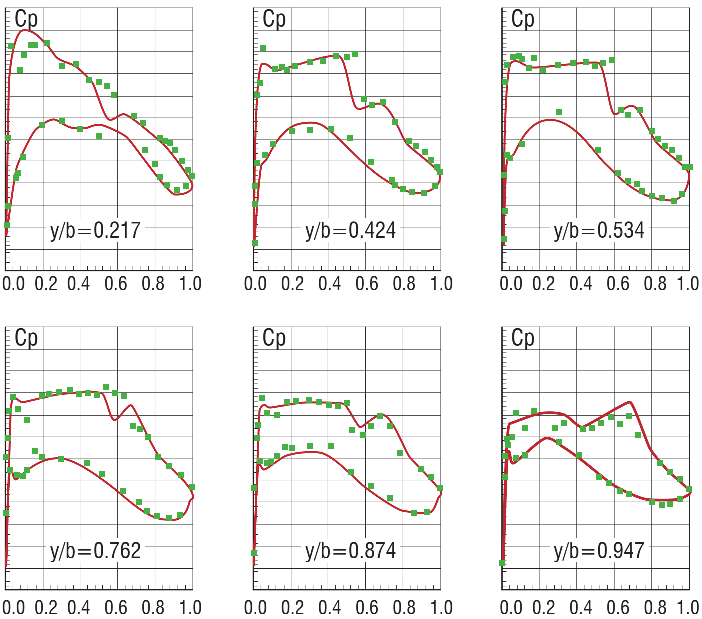

Figure 18 – Pressure coefficient distributions in several wing sections compared to flight measurements

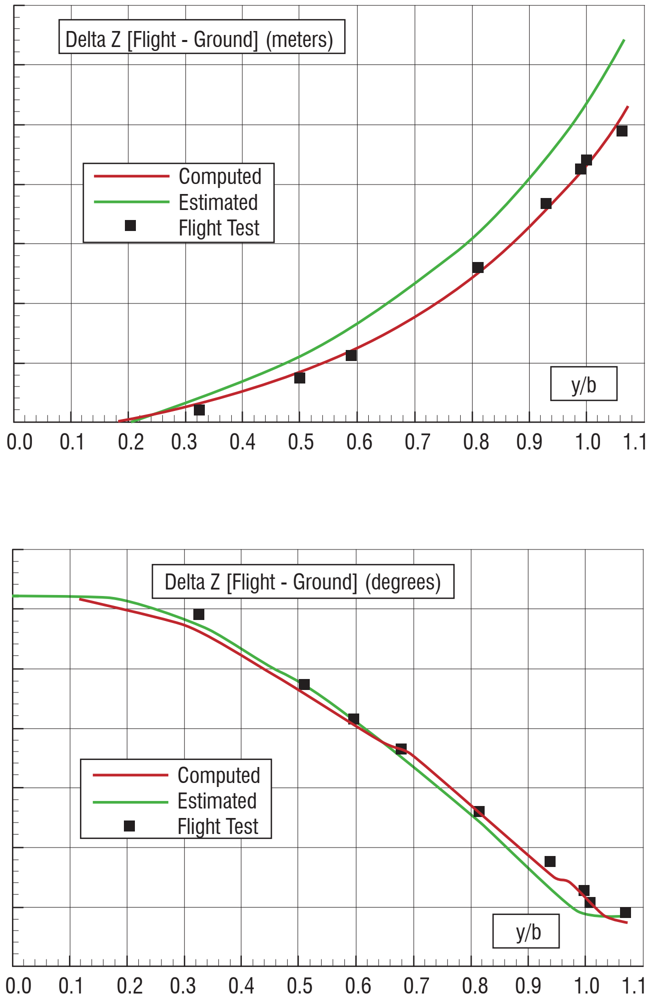

Figure 19 – Spanwise evolutions of vertical bending and twist deformations compared to flight measurements

Axial compressor aeroelastic stability analysis

One major issue in the aeronautical turbofan design process is to ensure engine safety over its entire operating range. The design process must therefore include flutter clearance procedures. During the 80's and 90's, linear unsteady methods were widely used in the subsonic and supersonic regimes to analyze the occurrence of flutter on aeronautical structures, and they are still used as an industrial design tool. However, the design of many of today's aeronautical structures requires a better understanding of the steady and unsteady aerodynamic field, especially in the case of the transonic regime where strong non-linearities like shocks and boundary layers may occur. RANS and URANS simulations are now more and more commonly used for such purposes, at a much higher computational cost. Moreover, in the field of turbomachine aeroelasticity, additional complexities must be considered due to the effect of rotation and cyclic periodicity which leads to complex unsteady aerodynamic flows.

A numerical study was carried out at Onera (Aeroelasticity and Structural Dynamics Department) to analyze the aero-elastic stability of the compressor wide chord fan wheel model of a civil transport aircraft engine [17] with an unsteady Navier-Stokes approach. The objective of such simulations is to extract the aeroelastic damping of the structural modes of vibration for several operating points of the engine, in order to evaluate the dynamic aeroelastic stability of the fluid-structure coupled system.

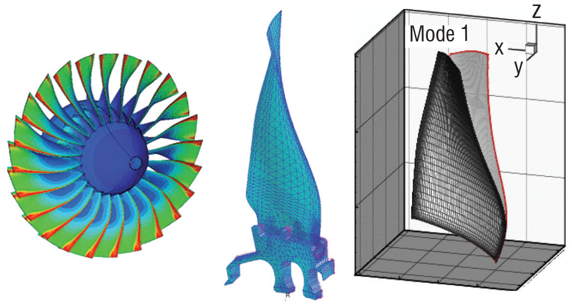

Figure 20 – Aerodynamic model - Structural fan model - First bending mode shape

The industrial fan model implemented for this study is a 24-blade wheel (figure 20). Several operating points of interest at 70 % of the nominal speed were investigated in the aeroelastic analysis, ranging from low compression up to near stall cases.

The dynamic structural behavior of the fan is represented by a finite element structural model made of roughly 50,000 grid nodes. Cyclic symmetry boundary conditions are defined at the disc sector boundaries. Complex modal bases are computed for various inter-blade phase angle values, taking into account the rotation effects of centrifugal stiffening and the gyroscopic damping.

Several aerodynamic modeling approaches have been considered. According to the cyclic periodicity of the system, single channel modeling is possible, thanks to the use of periodic boundary conditions. However, in order to take into account the incidence, distortion at inlet or geometrical or structural disturbances, it may still be necessary to model the entire 360° wheel.

In the first case, a single channel of the engine is represented using a 4 block and 0.8 10^6 cell Navier-Stokes structured grid. Steady and unsteady flows are computed using the Spalart-Allmaras turbulence model and the multi-grid convergence acceleration technique. In the second approach, a complete 360°, 24-blade model was built, leading to a 60 structured block grid counting about 20 10^6 cells.

Unsteady harmonic forced motion aeroelastic simulations were performed in order to get the generalized aerodynamic forces necessary to analyze the aeroelastic stability of the fan in its operating domain. These simulations were carried out using the URANS/dual time stepping classical approach (DTS), for both single sector and 360° models. Harmonic balance techniques (TSM) [18] are also now available and have been implemented and compared to the URANS results.

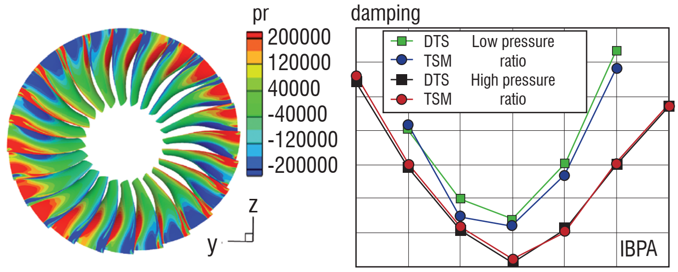

Figure 21 – Unsteady pressure harmonic analysis – Aeroelastic damping versus inter-blade phase angle

Figure 21 presents the evolution of the aeroelastic damping of the first bending mode, for both methods, and two operating points. A minimum aeroelastic damping is obtained for critical values of the inter-blade phase angle for near stall operating conditions. Such simulations are now implemented by the SAFRAN group for the evaluation of the aeroelastic stability of axial and centrifugal compressors.

Aero-acoustics

Over the past few years, the use of CFD has been intensified for noise prediction and reduction. Among the on-going Onera areas of activity, we can cite aerodynamic noise of high-lift devices and landing gears for transport aircraft, jet noise of turbofan engines, and noise produced by propellers and helicopter rotors. Since the full aero-acoustic simulation of such configurations is out of reach, the most common strategy involves coupling of the simulation of unsteady near field aerodynamic sources and acoustic propagation in the far field, with the near field noise sources being predicted by the use of Euler, URANS or RANS/LES approaches. The Blade Vortex Interaction noise, typical of helicopter applications, has been selected in this paper to illustrate the current CFD capabilities.

Major research efforts were made for prediction of Blade Vortex Interaction noise, which remains the primary source of noise pollution in usual descent flight conditions. For many years the CFD simulation of this phenomenon, consisting of the interaction between the blades and the rotor wake, remained an important challenge as it required accurate capture and long conservation of the blade tip vortex during the rotor revolution. Within the framework of the French-German program SHANEL, the baseline HART configuration of the BO105 rotor in descent flight was used to test and validate recent developments of the *elsA* code [19].

In a first step, an assumption of rigid blades is made and there is no coupling between the CFD and the rotor dynamics during the rotation (the kinematics of the blades are prescribed). In order to take into account the blade motion, the Chimera technique is used to overlap the different meshes. The effect of the blade grid refinement and of two different approaches for the background mesh is studied. A multi-block grid has been “manually” realized with different spatial resolutions (for a blade chord c, the coarse grid corresponds to Δh=0.3c, the standard one to Δh=0.15c and the fine one to Δh=0.075c). A specific solver for Cartesian grids (named Cassiopée) has been developed at Onera. It generates and automatically adapts Cartesian background grids around a body. Several inviscid unsteady computations have been realized to study the effect of timestep, blade grid or background grid resolutions and to test high-order space schemes. On the finest mesh (figure 22), the wake capture is quite accurate with a strong vortex intensity kept during about 1.5 revolutions, which is necessary for the interaction with the following blades.

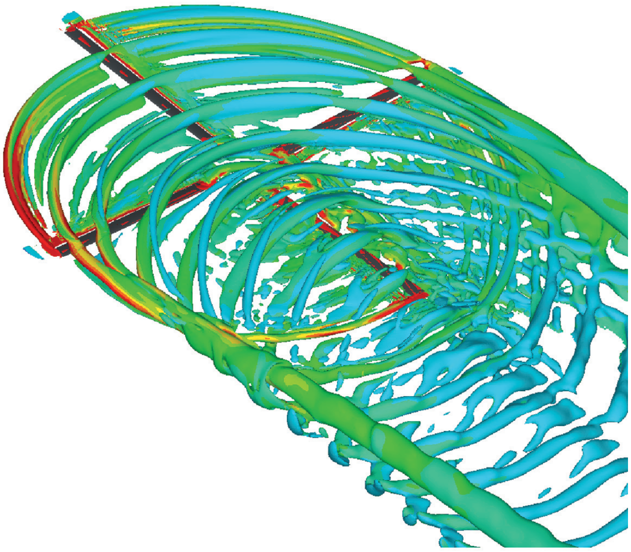

Figure 22 – Wake structure of the BO105 rotor in descent flight. Fine grid resolution

Figure 23 shows the evolution of the sectional lift coefficient C_zM^2 at r/R=0.87 on the advancing side. The multi-block background mesh resolutions are compared: for the coarse grid, no BVI oscillation is present. For the standard mesh (8 10^6 nodes), the most important peaks are simulated. Finally, the amplitude and the phase of all oscillations are improved with the finest mesh. Similar comparisons have been made for different numerical schemes tested on the Cartesian coarse grid. The order of both scheme and Chimera interpolations has been studied. The third order in spatial scheme noticeably improves the solution, as some BVI oscillations appear even on the standard mesh. Moreover, matrix dissipation of the Jameson scheme yields a solution comparable to the one obtained on the fine mesh (30 10^6 nodes).

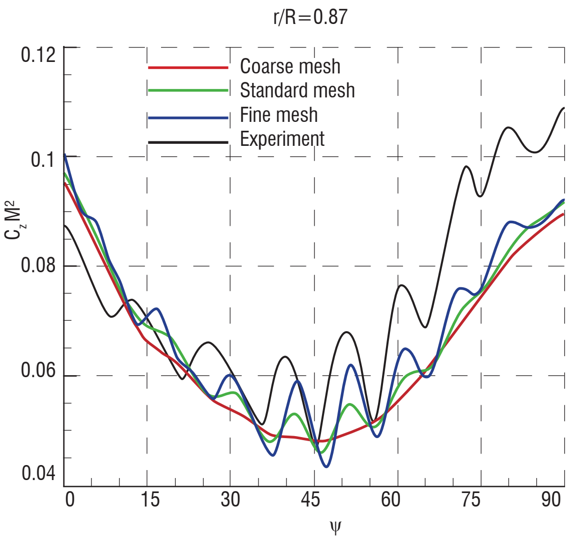

Figure 23 – Influence of mesh refinement on airload fluctuations: Advancing side Blade-Vortex-Interaction peaks

An acoustic post-processing of these CFD results has been performed by the multi-application acoustic code KIM using an integral method developed at the Onera Computational Fluid Dynamics and Aero-acoustics Department. There is a significant improvement of the noise level prediction for both the advancing and retreating blade sides, while passing from the standard to the fine mesh. The maximum noise level is increased by 7 dB and the under-estimation is reduced to 3.5 dB when comparing with the corresponding measured level. These results are very encouraging for BVI capture and understanding. Future steps in this study will consist of taking viscous effects into account and performing the coupling between aerodynamics and dynamics for a better prediction of aero-elastic effects.

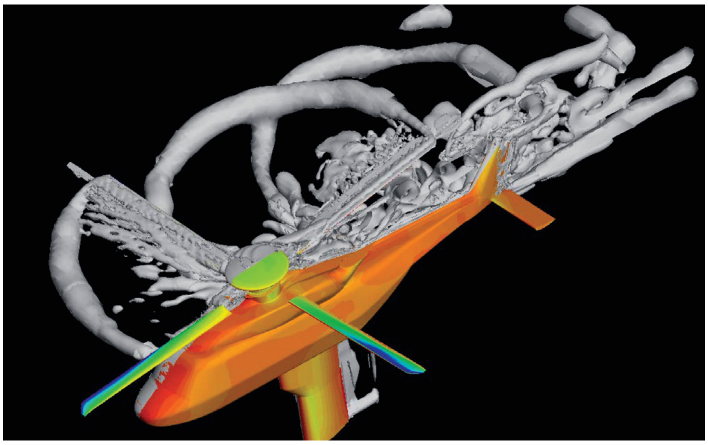

Figure 24 – Simulation of a complete helicopter configuration (including main and tail rotors) by a Chimera Cartesian technique

Another challenging application would be the prediction of the tone noise radiated by a complete configuration, such as the one studied in the GoAhead project and illustrated in figure 24.

Thermal effects

The prediction of aero thermal effects on industrial turbines is a key aspect in the dimensioning of the mechanical parts located downstream of the combustion chamber outlet. A significant effort has been made over the past few years to validate the *elsA* code for aero-thermal applications, especially in the TATEF2 European project [20].

Time accurate simulations of the TATEF2 one stage HP turbine were carried out with *elsA* using the phase-lagged (Chorochronic) technique which allows for reduction of the computational domain to one channel of the stator and the rotor.

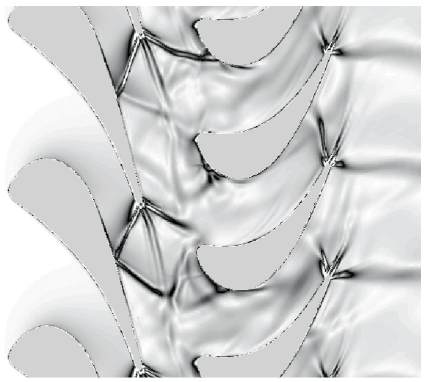

Figure 25 – Visualization of density gradients from the simulation of the Tatef2-VKI HP turbine

The configuration is characterized by the presence of strong shocks appearing on the VKI highly loaded turbine, as illustrated in figure 25 where the trailing-edge shock impact of the neighboring blades can be clearly identified.

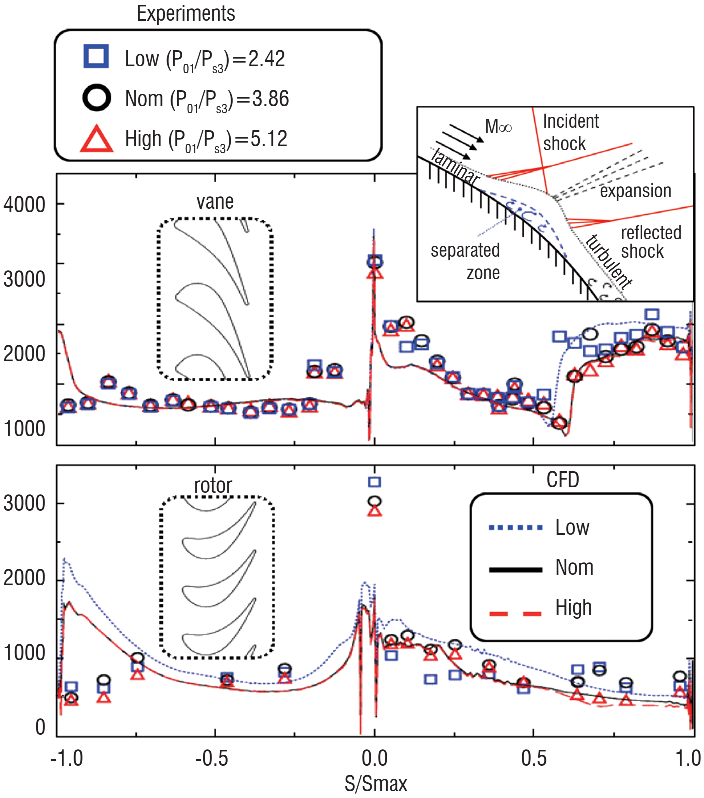

Figure 26 – Comparison between measured and calculated Nusselt number distributions (Tatef2-VKI HP turbine)

Figure 26 compares the Nusselt number distribution on the stator and the rotor for 3 different pressure ratios (Low, Nom and High). A good correlation is obtained, especially on the stator, where we can observe on the suction side the impact of the shock from the neighboring blade generating a laminar-turbulent boundary layer transition associated with an increase of heat fluxes. The improvement of such simulations would require more adapted turbulent and transition models, which is certainly a key topic of research in the near future.

Performance improvement

Environmental factors, such as fuel consumption and air pollution, will play an important role in the future growth of the transportation system. It is imperative to improve vehicle performance. For this reason, the use of design techniques such as numerical optimization is becoming increasingly attractive. Three applications of optimization techniques are presented in this section: pylon and winglet optimization for civil transport aircraft, and helicopter blade optimization. The three applications are based on the use of gradient methods and the discrete adjoint technique which is implemented in the *elsA* software.

Optimization

Pylon Optimization

The increasing size of modern aircraft engines with high by-pass ratios leads to increasing complexity of engine integration under the wing. For engine installation design, the use of the numerical optimization approach is a straightforward way to deal with the numerous aerodynamic and geometrical constraints. Furthermore, as the drag and weight penalties are of the same order of magnitude, Multi-Disciplinary Optimization could be an efficient approach to take both Aerodynamics and Structural Mechanics into account during the design [21].

As an example, the application of a hierarchical optimization for engine pylon design carried out in the VIVACE European project is presented in this section. The design of the outer board pylon of a large transport aircraft is examined in cruise conditions M=0.85, Re=20 10^6.

Three parameters identified as having an impact on both disciplines are considered at the higher level:

- X the variation of longitudinal position of the engine;
- Z the variation of vertical position of the engine;
- W the variation of the pylon width.

The optimization at the higher level is carried out thanks to surrogate models. This approach requires that configurations be sampled in the high level design space and optimized on the disciplinary level by varying low level parameters.

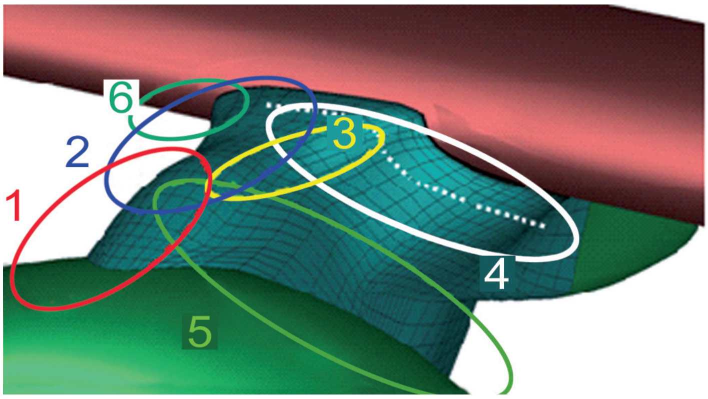

Figure 27 – Design parameters for the aerodynamic optimization of the outer pylon

The surrogate model for Aerodynamics is built with 9 samples. Each of them undergoes aerodynamic optimization carried out by a gradient method. At this lower level, parameters deal with the shape of the aerodynamic fairings as shown in figure 27. The parameterization considers 17 bumps spread on the pylon in different areas. The bumps are defined with Hicks-Henne functions in the direction of the flow whereas a cubic spline interpolation is used in the transverse direction.

In order to capture the complex transonic flow during the optimization process, the RANS approach was considered but the boundary layer was only computed accurately around the wing and the outer pylon. The corresponding mesh has 1.5 10^6 nodes.

Box 3 - Adjoint approach

Shape optimization aims at minimizing an objective function J while satisfying inequality on constraint functions G_k $(Gk \leq 0 \;\; k \in [1,nc])$. In the framework of CFD-based optimization, all functions depend on a vector of design parameters $\alpha=(\alpha_1, \alpha_2, ..., \alpha_{np})$, through the volume mesh, X, and the flow field, W (that is $J(\alpha)=J(W(\alpha),X(\alpha))$, $G_k(\alpha) = G_k(W(\alpha)X(\alpha)))$ which are linked by the discrete equations for fluid dynamics: $R(W(\alpha),X(\alpha))=0$. Most often, the number of functions of interest is much smaller than the number of design parameters $(1+nc<<n_p)$.

The derivatives of the objective function and the active constraints (i.e. reaching their null bound) at the current shape represent important information for doing the optimization. These derivatives can be computed by a non-intuitive method, the adjoint vector method, whose cost is almost independent of n_p, the number of design parameters, contrary to all simpler methods.

A detailed presentation of the method, in particular a discussion about how to get not only a low CPU cost, but also low memory requirements can be found for example in [22].

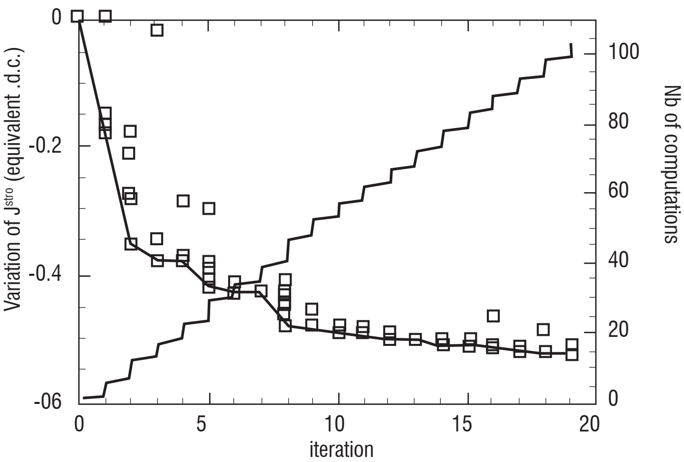

Figure 28 – Convergence of the aerodynamic optimization.

The selected optimization method requires knowledge of the gradient of the objective function which is computed by use of the RANS discrete adjoint approach implemented in the *elsA* software. To qualify the accuracy of the gradient predicted by the adjoint method, it was compared with a gradient obtained with finite differences on six design parameters controlling the height of six Hicks-Henne bumps. The agreement is moderately accurate for the dominant components, with a relative error in the 5-30% range. Keeping in mind the difficulty in deriving a finite difference gradient strictly independently of the chosen step, this was considered satisfactory enough for the purposes of the study.

Figure 28 presents the convergence of the aerodynamic optimization for one configuration. The results are satisfactory with most of the drag gain achieved with a few optimization iterations. After optimizing the configurations defined by the 9 high-level parameters, the aerodynamic response surface was established. The main trends obtained were the following:

- The drag is decreased when the engine is moved upstream;
- A wider pylon seems to decrease the drag in the investigated width range;
- The sensitivity of drag with respect to the Z variable is low.

The elaboration of this structural response surface will not be depicted in this section. Gathering information from the structure and aerodynamic surrogate models allows us to derive response surfaces for the multi-disciplinary problem.

This example has shown that an MDO approach could be used to reduce the number of design loops between disciplines. The local aerodynamic optimizations have been carried out with a gradient-based technique relying on the efficient adjoint approach implemented in *elsA* software for viscous flows.

Winglet optimization

The second application presented in this section focuses on the design of an integrated winglet for a civil transport aircraft. The design of such a wing-tip device is mainly driven by two disciplines, aerodynamics and structures [23]. For a fixed wing span, the use of an integrated winglet offers cruise performance improvements thanks to a lift-induced drag reduction. However, these aerodynamic characteristic improvements induce an increased structural weight of the wing due to the additional aerodynamic bending moment.

The winglet was designed by numerical optimization considering three design parameters: the winglet height, its leading edge sweep angle and its tip aerodynamic twist. All the aerodynamic analyses were carried out with the *elsA* software in the RANS mode with the Spalart Allmaras turbulence model. The different grids needed during the optimization were produced with an in-house analytical mesh deformation procedure applied to the baseline configuration grid produced with the ANSYS-ICEM-CFD mesh generator (400,000 nodes). The structural modeling used in this study, defined by the Aeroelasticity and Structural Dynamics Department, is based on the MSC-NASTRAN Finite Element software. The NASTRAN optimization capabilities were used to size the wing box structure by minimizing the structural weight of the wing. The aerodynamic loads of a 2.5 g maneuver have been used to stress the structure in this structural sizing process. The total wing weight has been estimated with the previous procedure for a set of different winglet geometries sampling the intended design space. The different results were used to build a surrogate model of the variation of the total wing weight.

The optimization problem has been formulated as a minimization problem of an aero-structure composite objective function defined as:

$$J(\alpha)=\Delta CDcruise(\alpha)+ \Delta weight(\alpha)/k$$

With α being the design variables, $\Delta CDcruise$ the variation of the aerodynamic drag coefficient in cruise conditions, $\Delta weight$ the variation of the structural weight of the complete wing structure with respect to the baseline configuration and k a trade-off coefficient.

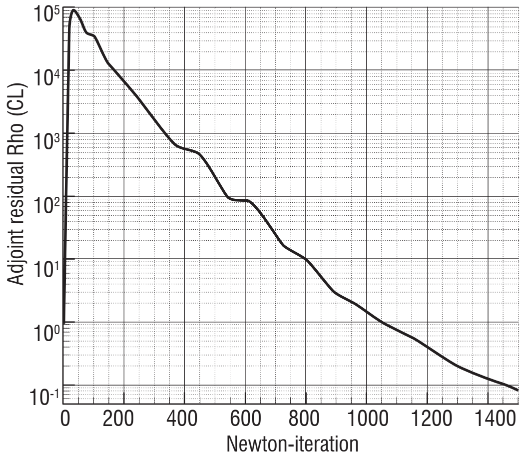

Figure 29 – Convergence of the Adjoint in transonic viscous flow

The optimization was based on the use of the DAKOTA optimization toolkit and the gradient optimizer CONMIN implementing the method of the feasible directions. The gradient of cruise lift and drag were computed by the Adjoint technique offered by the *elsA* software. As an example, figure 29 presents the good convergence of the adjoint residual versus the Newton-iterations (first component of the lift function adjoint). The aero-structural optimization was conducted at M=0.82 and the optimization convergence was obtained in 14 gradient iterations. The constraints on the lift coefficients in cruise (CL>0.5 at M=0.82) and maneuver conditions (CL>0.7 at M=0.60) are both satisfied at convergence while the final design yields a reduction of the aero-structural objective function J of about 40 equivalent-drag counts. The overall performance increase is obtained thanks to a reduction in the wing root bending moment of more than 1%, which allows for a structural weight reduction while the cruise drag is increased by about one count. The geometry of the optimized winglet is presented and compared to the baseline configuration in figure 30.

The presented work illustrates the possibility of evolving an aerodynamic optimization into a multi-disciplinary optimization where the additional discipline (structure) is taken into account using surrogate models. It has also demonstrated, for a realistic application, the ability of the *elsA* software to supply gradients thanks to the adjoint technique, which drastically reduces the computation time of the optimization process.

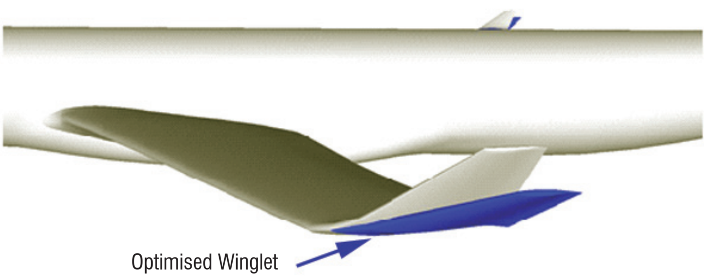

Figure 30 – Shapes of the reference and optimized winglets

Helicopter blade optimization

Aerodynamic shape optimization using gradient-based methods with an adjoint solver has mainly been used for fixed wing aircraft applications and very rarely for rotating wings. One reason is that simulating the multi-disciplinary unsteady problem with CFD is already complex, even without optimization. However, because helicopter hover flight can be described as a steady flow in the relative coordinate system, optimizing a helicopter rotor blade in hover using the descent method with approximation by the adjoint formulation of the gradients can be very attractive, since the computational cost remains almost insensitive to the number of shape parameters. Specific developments to adapt the adjoint formulation in *elsA* to rotating blades have been done in the framework of a thesis [24].

In a first step, the method has been validated by solving some academic problems, such as the well-known problem of geometric twist optimization. More complex applications were treated, for example by trying to optimize the hover efficiency (figure of merit FM) of the Onera ERATO blade [25], without any constraints.

The set of shape parameters retained for this optimization allows for modifications of the blade twist, chord and sweep distributions along the blade span, with each geometrical law being described by 8 Bezier control points. The collective pitch is also added as a design variable, which brings the total number of parameters to 25. Seven iterations of the optimizer were necessary, involving 31 flow solver solutions and 7 adjoint system calls, to find a local minimum.

a)

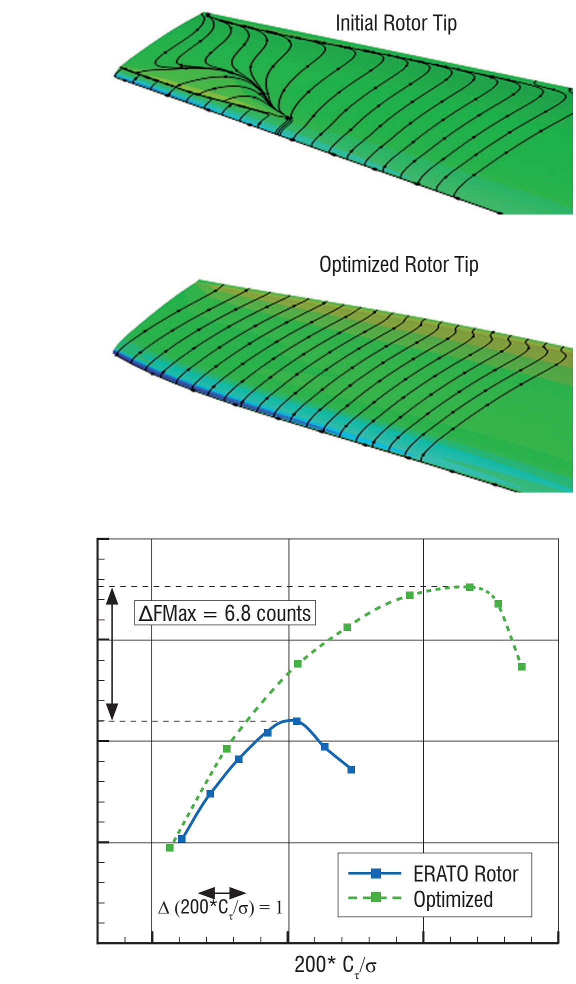

b)

Figure 31 – Optimization of helicopter rotor blade in hover flight. On a), streamlines on the initial and optimized blades. On b), improvement on the Figure of Merit

The Figure of Merit (FM) has been improved by 6.8 counts, together with an extension of the maximum take-off weight (figure 31). The optimized shape allows for suppression of the leading-edge shock recompression and flow separation near the blade tip, for a given collective pitch angle, as shown in the left part of figure 31. For this shape optimization problem, it is worth noting that the use of the adjoint method has divided the cost of sensitivity computations by a factor of 12 in comparison with the first order finite difference method.

The adjoint formulation implemented in *elsA* allows optimizations of helicopter rotors in steady conditions with an interesting design space to be investigated. The simultaneous optimization of hover efficiency and forward flight performance is a challenging topic that will require further algorithmic developments in the future.

Control of Flow Separation

Flow control is unanimously regarded as a key evolution, offering new solutions for performance maximization of existing designs, and, more broadly, the development of new concepts, in which separation control could be used in a multi-disciplinary approach, fully integrated with the initial screening and conception phases. Among the investigated flow control techniques, the most promising ones are the following:

- Passive, macro and sub-boundary layer vortex generators;
- Active, air-jet vortex generators;
- Active, pulsed and synthetic jets.

Three examples of applications have been selected in this section: control of the buffet phenomenon, separation control for helicopter fuselages, and suction and blowing in turbomachinery.

Control of the buffet separation

Flow control can be applied to transonic configurations in order to reduce drag and increase separation margins. In particular, the postponement of buffet onset with flow control technologies could lead to a more efficient aircraft having a smaller wing surface. This is why Onera launched a research program aiming at achieving buffet control using either an open or a closed-loop approach. The test was carried out in the S3Ch research wind tunnel of the Meudon centre to determine the efficiency of several control devices (VGs, AJVGs, pulsed jets) that were previously defined with CFD parametric studies. RANS and URANS approaches were used to assess the 3D model and to optimize the actuator characteristics (position, geometry, flow rates). The experimental results have shown that mechanical VGs, fluidic VGs and pulsed fluidic VGs were able to suppress the massive flow separation which occurs without control between the shock foot and over the trailing edge area which is at the origin of the buffet phenomenon [26].

For passive devices, the simulation of the control effect can be done by meshing the VG's geometry. However, strong limitations can appear in terms of mesh size and computational time when complex geometries such as engine installations are being considered. That is why the Bender et al. VG model [27] has been implemented in the *elsA* software and assessed at Onera [28]. Both approaches allow the intensity of the VG vortices to be well simulated while it turns out that the VG model is the most practical method for carrying out parametric studies.

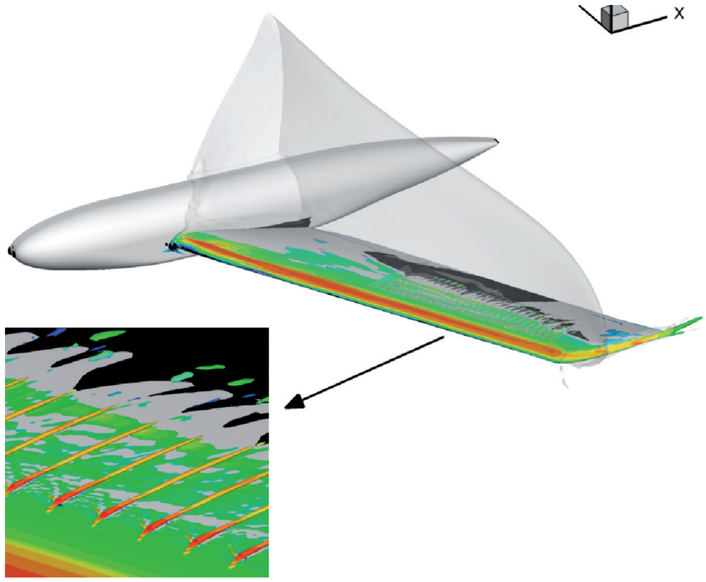

Figure 32 – Q-criterion iso-surface colored by Mach number showing the streamwise vortices created by the co-rotating mechanical VGs

Figure 32 presents the wing body configuration considered in this project and displays the results of a RANS simulation carried out with the VG devices installed on the outer part of the wing. The effects of the VGs are computed with the Bender et al. model and the computed flow is visualized by a Q-criterion iso-surface colored by the Mach number, the iso-surface M=1, and the separated zone in black. The streamwise vortices created by the co-rotating mechanical VGs are clearly visible. Small separated zones at the shock foot between the streamwise vortices are also visible, as in the experiment.

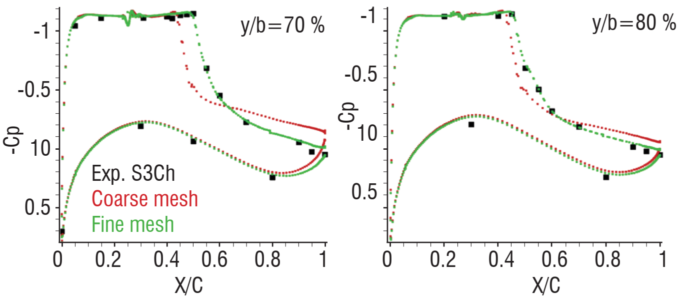

Figure 33 – Wall pressure distributions for the configuration with the co-rotating mechanical VGs

The wall pressure distributions for the controlled flow with mechanical co-rotating VGs are shown in figure 33 for two spanwise sections. The strong separation which is present on the reference configuration has been removed by the VGs. The agreement between the experimental data and the numerical simulation is very good, but with the fine mesh only (27 10^6 nodes). Good correlations have also been obtained with the fluidic VGs, taking advantage of the Chimera technique. The good quantitative agreement exhibited by the comparisons between simulations and experiment allows complex flow control applications with the *elsA* software to be investigated.

Separation control for helicopter fuselage

It has often been noted that the cruise drag of a rotary-wing aircraft is an order of magnitude higher than the cruise drag of a fixed-wing aircraft of the same gross weight. Function, or mission, drives the fuselage design of a rotary-wing aircraft more than aerodynamics. Accordingly, rotary-wing aircraft tend to have more bluff-body characteristics with the flow around the aft end of the fuselage typically being dominated by massive flow separation. This results not only in a large quantity of pressure drag, but also in a wake that tends to become unsteady. This, in turn, introduces undesirable, unsteady loads to the tail boom, stabilizers and tail rotor. An effort has been undertaken to study this problem on a generic fuselage with the goal of reducing the fuselage drag, while minimizing the effects of adverse lift. The drag reduction is to be achieved by the application of active flow control to the separated flow at the aft end of the fuselage.

Within the framework of the Cleansky GRC2 project, Onera has chosen to work on the ASF2 fuselage tested in the 80-90s in the F2 wind-tunnel. The first step was to perform CFD calculations of the uncontrolled flow on this geometry and to compare the results with experimental data. For steady computation, a low-Mach preconditioning method was used to enhance convergence and drag prediction accuracy, which was necessary for the low speed configurations studied here ($M<0.1$). In the case of unsteady computations, a Newton method based on the Gear algorithm was used. Finally, the k-ω Kok turbulence model [29] was chosen among the various models implemented in *elsA*. The initial mesh was about 4.8 10^6 nodes and was refined in the separation area.

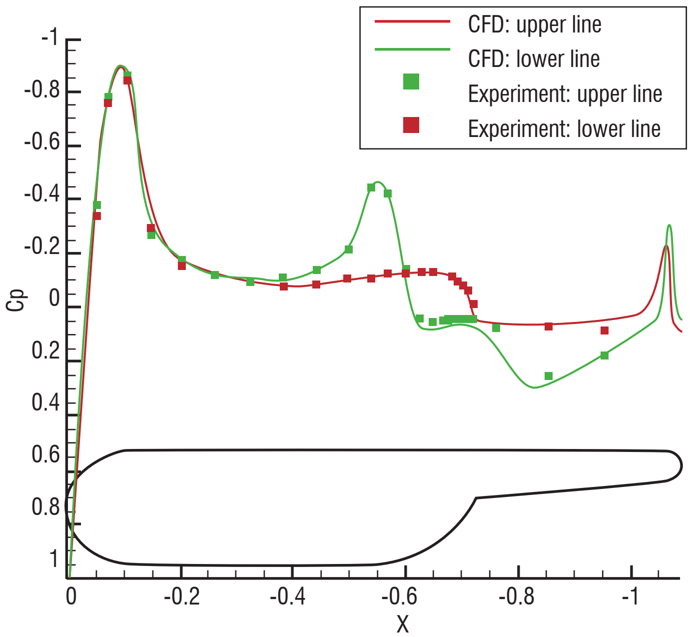

Figure 34 – Comparison of pressure distribution of the ASF2 fuselage. No incidence, no flow control

Figure 34 shows that the pressure distribution is very well predicted by the simulations, including the pressure plateau in the bottom part of the fuselage (ramp area), where massive flow separation occurs. Until now, the most promising results have been obtained by applying synthetic jets in order to control the flow separation in the ramp area. 4 slots were placed in order to "surround" the detached area (figure 35).

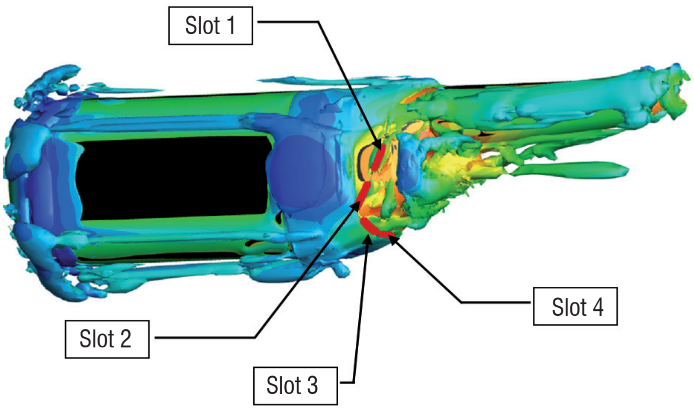

Figure 35 – Location of the 4 slots and visualization of the flow field on the ASF2 fuselage with flow control

When the 4 jets are in phase, whatever the tested condition, the drag coefficient of the fuselage increases. The interesting result is that out-of-phase jets (vertical slots out-of phase, and same for horizontal slots) allow for reduction of the unsteady load fluctuations, and also the mean drag value, as illustrated in figure 36. This reduction can reach 14% with this 4 out-of-phase jet configuration, with a C_μ coefficient of 2.1% and a non-dimensioned actuation frequency $F^+\approx 1$, and jets oriented at 20° with respect to the surface normal.

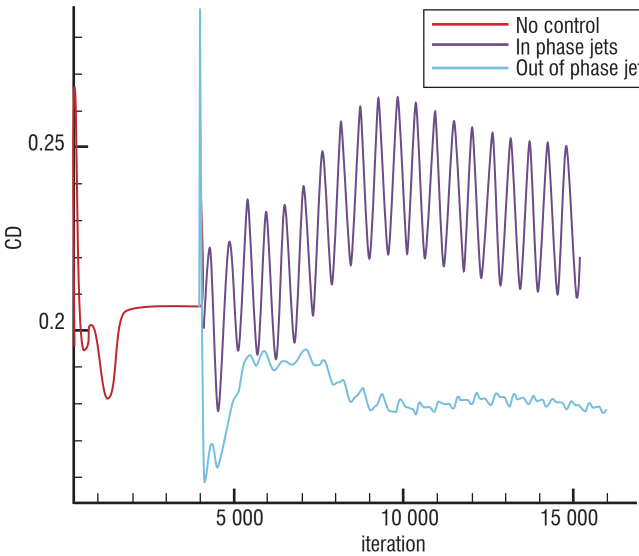

Figure 36 – Influence of synthetic jets on the helicopter ASF2 fuselage drag coefficient

A detailed analysis of the vortex structures in the uncontrolled and controlled cases is underway in order to explain the physical phenomena involved and to try to find the best control strategy for blunt fuselage drag reduction.

Suction and blowing in turbomachinery

An efficient way to increase the pressure ratio of a compressor involves aspirating the viscous layers that can develop in the inter blade channels. This strategy has been evaluated for low pressure compressors, in the framework of a thesis [30], with the objective of reaching a deviation as large as 65° for a diffusion rate of 2. The strategy is to fix the separation point on the blade by creating a sudden diffusion and curvature variation: it is then easier to appropriately locate the suction device that can be placed just after the curvature modification.

The blading was defined using *elsA* calculations for an upstream Mach number equal to 0.7. The cascade was then defined, manufactured and tested at the LMFA for low speed conditions (M=0.12). Non-intrusive flow measurements using PIV are compared with predictions in figure 37. The suction rate required to reach a total flow re-attachment is estimated to be 3.3%. There is a very good correlation between the calculations and the measurements, especially in the case of aspiration where the diffusion is predicted with an accuracy of 6%. Although the target deviation was almost reached in the experiment (62.2° instead of 65°), some lateral separations lead to a diffusion of only 30%. The next step in this study would be to define a 3D aspirated compressor stage and test it for real Mach number conditions.

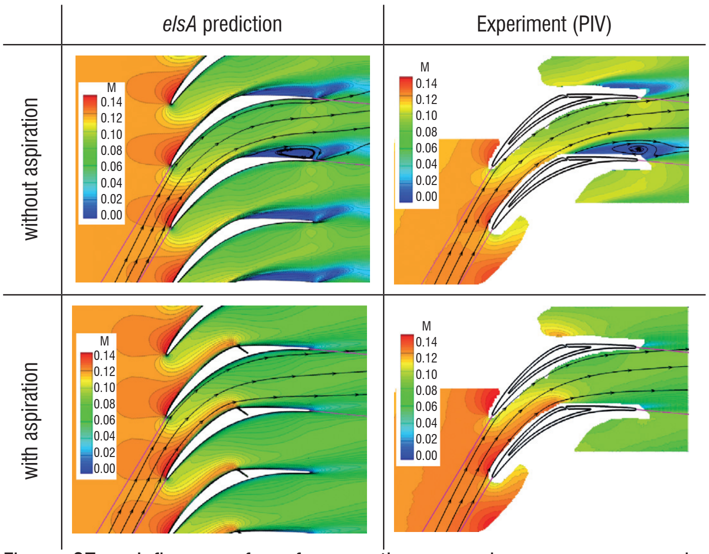

Figure 37 – Influence of surface suction on a low-pressure cascade. Comparison between calculations (left) and measurements (right)

New concepts

Flying wing

The aerodynamic design of modern transport aircraft is driven primarily by cruise performance and regulation considerations. Future environmental constraints will require significant reductions in emissions and noise pollution. Although the improvement in existing aircraft performance may provide a short-term answer to this problem, the development of radically novel configurations is likely to be required to meet the long-term improvement objective. The flying wing or blended wing body seems to be one of the most promising configurations for reaching efficiency higher than that of the current configurations.

For several years now, the Applied Aerodynamics Department of Onera has been working on flying wing configurations for large capacity transonic transport within the framework of national and European projects. Recently, a national research project AVECA was launched on Blended-Wing-Body configurations of smaller capacity in close cooperation with Airbus [31]. This project aimed at designing viable flying wing geometries in terms of aerodynamic cruise performance (M=0.85) while respecting longitudinal trimming and geometric constraints such as cabin or landing gear volumes.

In order to reach these objectives, the first step in the design consisted of redesigning the wing profiles using control points (B-splines) based on geometry deformation of several wing sections while keeping the planform of the configuration unchanged. The iterative design process was begun by modifying the inboard section, and progressively moving to the outer section of the configuration. The second step of the design involved optimizing the twist law of the outboard wing to improve the lift-to-drag ratio and the longitudinal trimming of the configuration at the design point.

To evaluate the aerodynamic performance of the various configurations during the design process, the Onera *elsA* software was used to carry out CFD computations on a Navier-Stokes structured mesh made up of 8.0 10^6 points, and the Onera far-field drag extraction code ffd72 was used to evaluate the total drag and to determine the drag components.

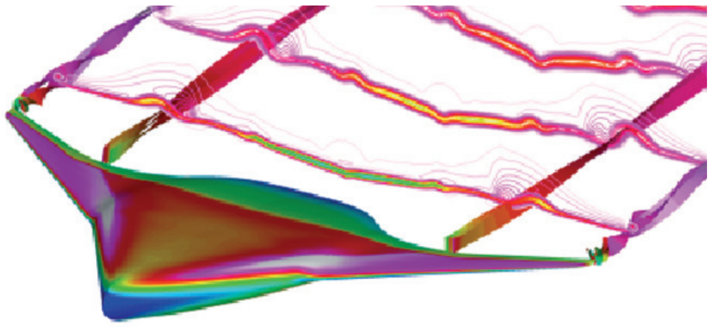

Figure 38 – Simulation on the AVECA flying wing configuration (M=0.87)

With this iterative strategy, very convincing results were obtained with an increase of the lift-to-drag ratio of 5% at the design point and of 19% at a higher Mach number (M=0.87 - figure 38). These gains are mainly due to a strong decrease of the wave and viscous drag components.

In the current AVECA project, the adjoint optimization method developed in the Onera *elsA* software will be used to automate the design process for flying wing configurations.

Supersonic business jet

Over the past few decades, several aircraft makers have investigated various concepts for a supersonic transport aircraft (SST). More recently, a small supersonic business jet concept was proposed and studied, particularly within the European project HISAC of the 6th R&D Framework Program. The HISAC project managed by Dassault-Aviation aims at establishing the technical feasibility of an environmentally-compliant, small-size supersonic transport aircraft. Several concepts such as low noise, long range and low sonic boom were investigated through CFD simulations and wind tunnel tests.

As far as the aerodynamics are concerned, Onera's contributions have focused on the determination of the aerodynamic characteristics, the prediction of the sonic boom, the aerodynamic and MDO optimizations and high-speed wind tunnel tests. As an example of the Onera work, figure 39 presents the results of a RANS simulation carried out with the *elsA* software for the reference configuration tested in the Onera S2MA wind tunnel. The multi-block mesh has 11 10^6 nodes and the nacelle is integrated with the wing body configuration thanks to the patched-grid technique. The aerodynamic conditions are a cruise Mach number of 1.6, an angle of attack of 5° and a lift coefficient of 0.2 (above the cruise lift coefficient). The streamlines point to the presence of the apex and wing kink vortices induced by the fuselage and the strong sweep of the inner wing. The correlation carried out with the wind tunnel results (balance and static pressures in two lines) shows good agreement.

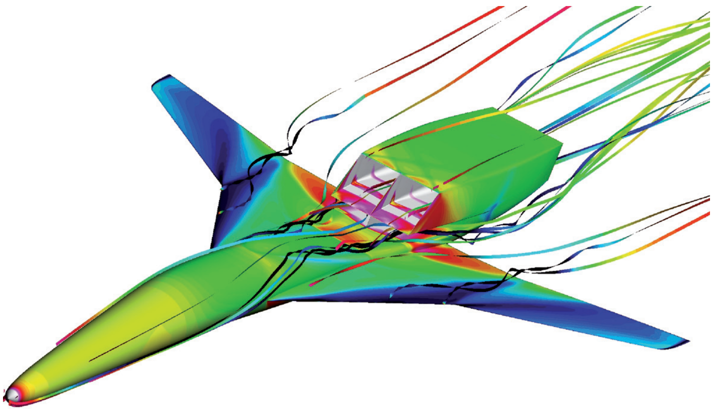

Figure 39 – Simulation of one of the HISAC business jet configurations

UCAV configuration

The Next generation of UCAV will be based on blended wing-body configuration with a moderate sweep angle. This kind of UCAV exhibits rather complex vortex-dominated flows when compared with highly swept delta wings. Due to the competition between the apex vortex and the wing tip vortex, these configurations exhibit strong pitch-up behavior at a relatively low angle of attack (~17°) and lateral instability that can lead to serious aerodynamic stability and control issues.

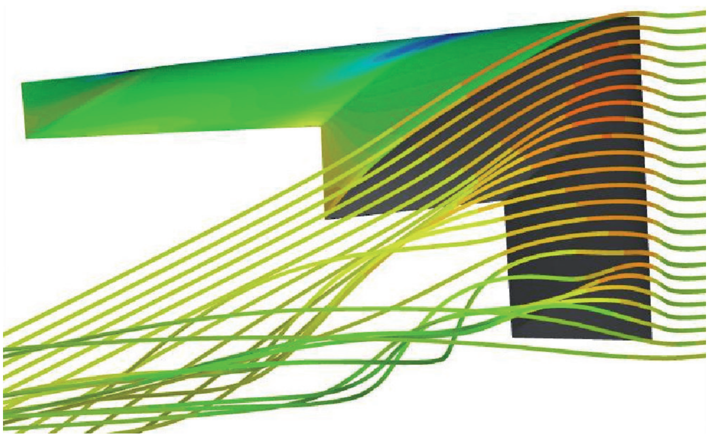

Figure 40 – Computed streamlines around the UCAV Configuration. M=0.14, Re=1.6 10^6, α=17°

For these reasons, the static and dynamic derivatives are being investigated for a representative UCAV with a CFD approach and compared to the experimental results. The configuration, named SACCON for Stability And Control CONfiguration, is a blended wing body with a moderate sweep angle (53°) defined for the purpose of an RTO project. The CFD approach is based on static computations to determine the static derivatives and on the ALE (Arbitrary Lagrangian Euler) method coupled to steady or unsteady computations to obtain the dynamic derivatives. The objectives are to compare the time-history of the pitching moment coefficient between experimental and unsteady simulation for a pitching oscillation.

Figure 40 shows the complexity of the flow obtained at high angles of attack using the Spalart Allmaras turbulence model. Two main vortices are clearly visible. When the angle of attack is increased, the tip vortex has a growing intensity and its position moves inboard. The displacement of the tip vortex along the leading edge is the origin of the pitch-up observed in the wind tunnel on this configuration. Ongoing activities are related to the use of advanced turbulence models such as EARSM and DRSM.

CROR

Counter-Rotating Open Rotors (CROR) represent an attractive alternative to conventional turbofan engines because of their reduced impact on the environment (fuel consumption reduction), as a consequence of their high by-pass ratio. The success of this concept will depend greatly on the noise levels radiated by the installed power plant system. The numerical simulation of a complete configuration through CFD is certainly very challenging, and can be envisaged in the near future. At present, Onera is involved together with Snecma and Airbus in many national and European projects that aim at validating the CFD methodologies that are well-suited for the prediction of accurate aerodynamic performance (take-off and cruise conditions), and for the prediction of aerodynamic noise sources.

The mixing-plane boundary condition developed in *elsA* for turbomachinery applications has been extended to propeller applications and allows for prediction of the steady aerodynamic performance of a CROR (figure 41), under the hypothesis of azimuthally averaged interactions between propellers. Its big advantage lies in its low CPU cost.

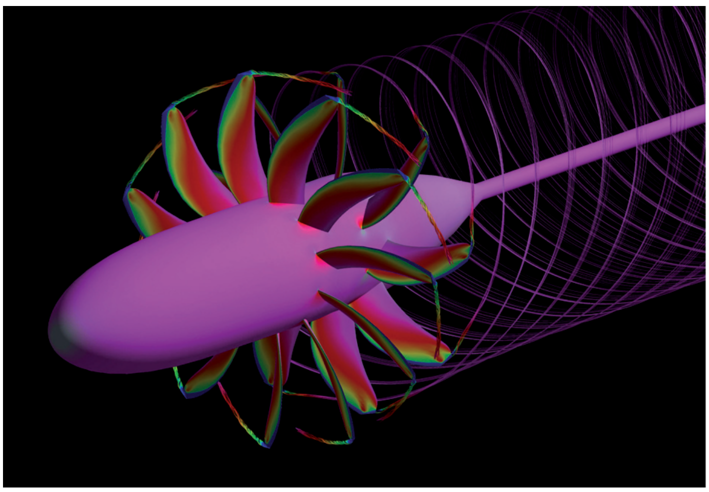

Figure 41 – Steady simulation of an Airbus CROR configuration using a mixing-plane interface between the propellers

The chorochronic conditions also developed for turbomachinery applications are an interesting and efficient way to have access to the time-accurate interactions between propellers, without needing to model all of the blades. Such simulations can predict the unsteady inputs required for an acoustic evaluation of the CROR, with moderate CPU cost; however, this method is only valid for an isolated CROR. Finally, when the objective is to study installation effects (incidence effects or interactions with the airframe), it is mandatory to model the whole configuration (360° calculation), leading to a very long CPU time (approximately ten times more than with the chorochronic method). In this case, the use of the Chimera functionalities available in the *elsA* software allows for simulations of the different rotating and fixed components of the configuration. The first applications of such a calculation have been done for an isolated CROR (figure 42), trying to better understand how well the aerodynamic interactions between the front propeller blade wakes and tip vortices and the aft propeller blades can be captured and how these interactions contribute to the radiated noise.

Further validation of the developed methodologies is necessary and is already planned for the near future, especially by comparing the numerical predictions with wind-tunnel test results.

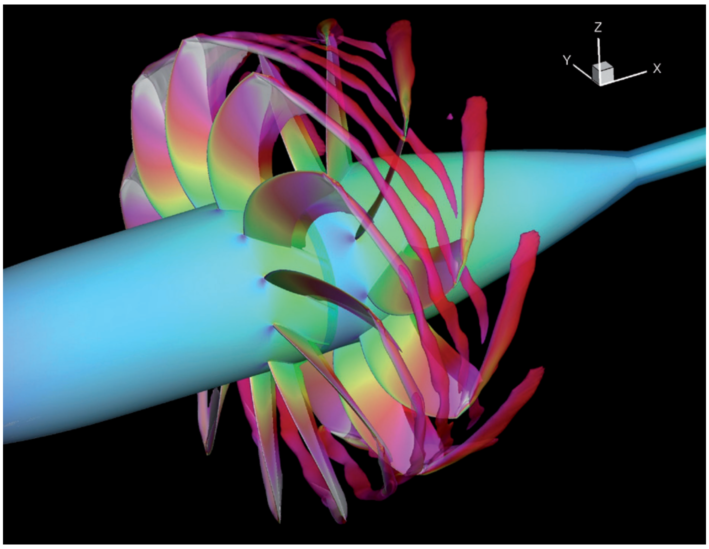

Figure 42 – Time-accurate 360° simulation of an Airbus CROR configuration using the Chimera technique

Tilt rotor

Tilt-rotors can be defined as hybrid aircraft, combining the advantage of hover capabilities specific to helicopters, with high speed capabilities similar to propeller driven aircraft. Most of the studies initiated in Europe over the past 6 years have been based on the ERICA concept proposed by AGUSTA, which is a tilt-rotor comprising a half tilt-wing design, which aims at reducing the rotor-wing interactions through a proper choice of the outer wing incidence depending on the flight condition.

In the NICETRIP European project, the use of CFD has allowed for the investigation of complex problems, two of which are detailed below. The first one is related to cabin noise, for which the *elsA* code has been used in order to predict the aerodynamic sources of the noise radiated by aircraft in cruise conditions [33]. Steady calculations of the isolated propeller have been compared to a time-accurate simulation of the installed configuration (figure 43): installation effects on the radiated noise have been quantified as large as 15 dBA. The origin of this large noise increase is the unsteady pressure fluctuations of the propeller blades due to the fuselage and wing tangential deviations in the propeller plane. Indeed, the peak-to-peak amplitude of the blade loading over one revolution can be as large as 3,000 N, compared with its average value of 1,825 N. The use of cyclic pitch, not actuated in the present simulations, may help in the future to reduce these fluctuations and then to decrease cabin noise.

The second activity has been to try to improve propeller cruise efficiency through optimization of the cuff shape (the cuff being the junction between the blade root and the spinner). Indeed, previous projects such as ADYN have shown that non-optimized cuff geometry can lead to a 20% reduction in cruise efficiency. Various concepts have been investigated to adapt the blade root geometry to the spinner, making intensive use of the complex Chimera functionalities available in *elsA* in order to compute geometry details including the modeling of one part of the internal spinner flow. The new proposed cuff geometry is expected to improve the cruise efficiency by more than 15% compared with the ADYN reference.

ERICA full scale - Cruise 330 kts
Q criteria iso-surface colored by vorticity magnitude
Skin pressure contour

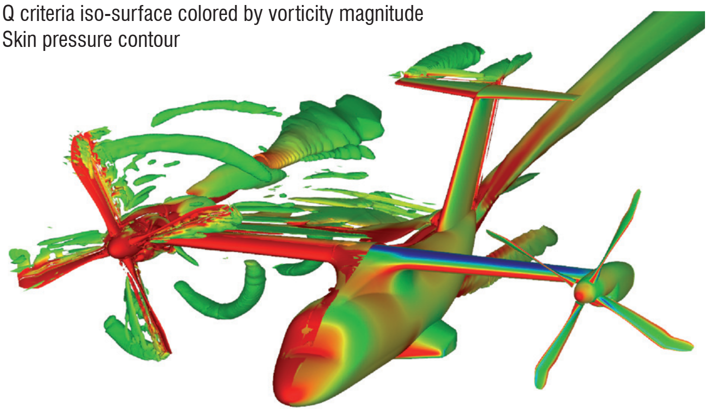

Figure 43 – Simulation of the ERICA tilt-rotor in cruise conditions

Conclusions and future work

The wide range of applications presented in this paper shows that the *elsA* software has reached a good level of maturity. It allows for carrying out RANS simulations with high CPU performance in parallel mode, and URANS and DES simulations to accurately predict unsteady aerodynamics. The ability to take into account several turbulence models and transition criteria and to perform accurate fluid/structure coupling simulations is also a strong asset for this software. The robustness of the RANS adjoint method for the calculation of sensitivities allows for complex 3D optimization.

Most of the applications presented have been assessed with aerodynamic databases established in Onera research wind tunnels. These databases are based on the use of advanced measurement techniques to quantify the flow on model surfaces or in the flow field: Pressure and Temperature Sensitive paints, Laser Doppler Velocimetry and Particle Image Velocimetry. Multi-physics databases are also needed to assess such complex simulations.

In order to cope with complex configurations, the development of a hybrid structured/unstructured mesh strategy will be added to the available high flexibility advanced techniques of multi-block structured, patched grid and overset capabilities (Chimera technique). The applications will be then oriented towards the simulation of the complex geometries with full details.

The drag extraction and optimization techniques will be extended to URANS capabilities. The simulations of detached flows currently carried out with the URANS and DES approaches will consider LES and DNS modes which will require new boundary conditions and refined meshes.

Multi-physics applications will also play a major role in the future with, in particular, the development of improved aero-elastic, aero-acoustic and aero-thermal simulations. These coupling applications will be eased by the adaptation of the *elsA* software to the massively parallel architectures of new computers ■

Acknowledgements

The authors would like to thank the French government agencies DGAC and DGA and the European Commission for funding some of the previous research studies.

The results presented have also been established through very good cooperation between various Onera departments: Applied Aerodynamics, Aeroelasticity and Structural Dynamics, Fundamental and Experimental Aerodynamics, Aerodynamics and Energetics Modeling, Computational Fluid Dynamics and Aero-acoustics.

Many researchers must be acknowledged for their works and their contributions to this paper: **S. Esquieu** and **D. Hue** for the drag prediction activities, **J.L. Hantrais-Gervois** and **O. Atinault** for the control surfaces, **F. Moens** for the high-lift configuration, **V. Brunet** and **S. Deck** for the buffet prediction and jet simulations, **M. Costes** and **A. Le Pape** for the dynamic stall activities, **P. Thorigny** for the store separation, **S. Mouton** for the CFD-wind tunnel synergy, **A. Dugeai** and **F. Sicot** for the axial compressor aeroelastic stability analysis, **T. Renaud** for the blade vortex interaction noise study, **L. Castillon** for the thermal study on the TATEF turbine, **S. Mouton** for the pylon optimization, **G. Carrier** for the winglet optimization, **A. Dumont** for the helicopter blade optimization, **J. Peter** for the contribution to the adjoint technique, **J. Dandois** for the control of buffet phenomenon, **C. Liénard** for the separation control on helicopter fuselage investigation, **L. Castillon**, **A. Godard** and **S. Burguburu** for the suction and blowing effects in turbo-machinery, **M. Méheut** for the flying wing configuration, **G. Carrier** for the supersonic business jet, **J.F. Leroy** for the UCAV configuration **B. Rodriguez** and **S. Burguburu** for the CROR configuration, **J. Decours** for the tilt-rotor study.

References

[1] L. CAMBIER, J.P. VEUILLOT - *Status of the elsA Software for Flow Simulation and Multi-disciplinary Applications*. 46th AIAA Aerospace Sciences Meeting and Exhibit, Reno, Nevada, AIAA2008-664, 7th to10th January 2008.
[2] D. HUE, S. ESQUIEU and M. GAZAIX - *Computational Drag and Moment Prediction of the DPW4 Configuration Using elsA.* AIAA conference, Chicago, June 2010.
[3] D. DESTARAC - *Far-field / Near-field Drag Balance and Applications of Drag Extraction in CFD. CFD-Based Aircraft Drag Prediction and Reduction*. Hampton, VA, 3th to 7th November 2003.
[4] J.-L. HANTRAIS-GERVOIS, A. LEPAGE, F. TERNOY, G. CARRAZ and G. JEANFAIVRE - *Assessment of Numerical Tools to Predict Control Surface Effectiveness.* AIAA Applied Aerodynamics Conference, Chicago, 28th June to 1st July 2010.
[5] J. CLIQUET, R. HOUDEVILLE, D. ARNAL - *Application of Laminar-Turbulent Transition Criteria in Navier-Stokes Computations*. AIAA Journal, Vol. 46, N° 5, May 2008.
[6] F. MOENS, J. PERRAUD, A. KRUMBEIN, T. TOULORGE, P. IANELLI, P. ELIASSON and A. HANIFI - *Transition Prediction and Impact on a Three Dimensional High-Lift Wing Configuration*. AIAA Journal, Vol.45, N° 5, pp 1751-1766, September-October 2008.
[7] V. BRUNET, P. MOLTON, H. BÉZARD, S. DECK and L. Jacquin - *A Joint Numerical and Experimental Study of the Jet of an Aircraft Engine Installation with Advanced Techniques*. 3rd European Conference for Aerospace Sciences, Versailles, July 2009.
[8] S. DECK - *Numerical Simulation of Transonic Buffet over a Supercritical Airfoil.* AIAA Journal, Vol. 43, N° 7, pp 1556-1566, 2005.
[9] P. SAGAUT, S. DECK and M. TERRACOL - *Multi-Scale and Multi-Resolution Approaches in Turbulence*. Imperial College Press, London, UK, 2006.
[10] P.R. SPALART, S. DECK, M.L. SHUR, K.D. SQUIRES, M. STRELETS and A. TRAVIN - *A New Version of Detached Eddy Simulation Resistant to Ambiguous Grid Densities*. Theoretical and Computational Fluid Dynamics, Vol. 20, pp 181-195, July 2006.
[11] S. DECK - *Zonal Detached Eddy Simulation of the Flow Around a High-Lift Configuration*. AIAA Journal, Vol. 43, N° 11, pp 2372-2384, 2005.
[12] P. SAGAUT and S. DECK - *Large Eddy Simulation for Aerodynamics: Status and Perspectives*. Phil. Trans. R. Soc. A., Vol. 367, pp 2849-2860, 2009.
[13] K. RICHTER, A. LE PAPE, T. KNOPP, M. COSTES, V. GLEIZE and A. Gardner - *Validation of Structured and Hybrid Methods for Improved Two-Dimensional Dynamic Stall Prediction*. 10th Onera-DLR Aerospace Symposium, Berlin, 6th to 8th October 2009.
[14] J.-J. HANTRAIS-GERVOIS, A. CARTIÉRI, S. MOUTON and J.-F. PIAT - *Empty Wind Tunnel Flow Field Computations*. International Journal of Engineering Systems Modeling and Simulation, Vol. 2, Nos 1/2, 2010.
[15] S. MOUTON - *Numerical Investigations of Model Support Interference in a Transonic Wind Tunnel.* 44e Colloque d'Aérodynamique Appliquée, Nantes, March 2009.
[16] P. GIRODROUX-LAVIGNE - *Progress in Steady/Unsteady Fluid-Structure Coupling with Navier-Stokes Equation*. International Forum on Aeroelasticity and Structural Dynamics, Munich, Germany, 28th June to 1st July 2005.
[17] A. DUGEAI - *Turbomachinery Aeroelastic Developments and Validations Using Onera elsA Solver*. International Forum on Aeroelasticity and Structural Dynamics, Stockholm, Sweden, 18th to 20th June 2007.
[18] G. DUFOUR, F. SICOT, G. PUIGT, C. LIAUZUN and A. DUGEAI - *Contrasting the Harmonic Balance and Linearized Methods for Oscillating-Flap Simulations.* AIAA Journal, Vol. 48, n°. 4, pp 788-797, April 2010.
[19] T. RENAUD, G. PEREZ, C. BENOIT, G. JEANFAIVRE and S. PÉRON - *Blade-Vortex Interaction Capture by CFD*. 34th European Rotorcraft Forum, Liverpool, 16th to 19th September 2008.

[20] G. PANIAGUA, T. YASA, A. DE LA LOMA, L. CASTILLON and T. COTON - *Unsteady Strong Shock Interactions in a Transonic Turbine. Experimental and Numerical Analysis*. J. of Propulsion and Power, Vol.24, N° 4, pp 722-731, 2008.
[21] S. MOUTON, J. LAURANCEAU and G. CARRIER - *Aerodynamic and Structural Optimization of Power-Plant Integration under a Wing of a Transport Aircraft.* 42^{e} Colloque d'Aérodynamique Appliquée AAAF, Sophia-Antipolis, 19^{th} to 21^{th} March 2007.
[22] J. E.V. PETER and R. P. DWIGHT - *Numerical Sensitivity Analysis for Aerodynamic Optimization: A Survey of Approaches*. Computers & Fluids, Vol. 39, 2010.
[23] G. CARRIER, S. MOUTON, M. MARCELET and C. BLONDEAU - *Towards Aerodynamic Design by Optimization of Transport Aircraft in a Multi-Disciplinary Context*. CEAS Conference 2007, Berlin, Germany, 10^{th} to 13^{th} September 2007.
[24] A. DUMONT, A. LE PAPE - *Aerodynamic Shape Optimization of Hovering Rotors Using a Discrete Adjoint of the RANS Equations*. 65^{th} American Helicopter Society Forum, Grapevine, 27^{th} to 29^{th} May 2009.
[25] J. PRIEUR, W. SPLETTSTOESSER - *ERATO - an Onera-DLR Cooperative Program on Aeroacoustic Rotor Optimization*. 25^{th} European Rotorcraft Forum, September 1999.
[26] J. DANDOIS, V. BRUNET, P. MOLTON, J. ABART, A. LEPAGE and F. TERNOY - *Buffet Control by Means of Mechanical and Fluidic Vortex Generators*. AIAA Paper 2010-4975, Chicago, 28^{th} June to 1^{st} July 2010.
[27] E.E. BENDER, B.H. ANDERSON and P.J. YAGLE - *Vortex Generator Modeling for Navier-Stokes Codes*, FEDSM 99-6919, July 1999.
[28] M. MEUNIER and V. BRUNET - *High-Lift Devices Performance Enhancement Using Mechanical and Air-Jet Vortex Generators*. AIAA Journal, Vol. 45, N° 6, pp 2049-2061, 2008.
[29] J.C. KOK - *Resolving the Dependence on Freestream Values for the k-w Turbulence Model*, AIAA Journal, Vol. 38, N° 7, pp 1292-1295, July 2000.
[30] A. GODARD, A. FOURMAUX, S. BURGUBURU and F. LEBOEUF - *Design Method of a Subsonic Aspirated Cascade*, ASME Turbo Expo 2008, Berlin, 9^{th} to 13^{th} June 2008.
[31] M. MÉHEUT, R. GRENON, G. CARRIER, M. DEFOS, M. DUFFAU - *Aerodynamic Design of Transonic Flying Wing Configurations*. CEAS/KATnet2 Conference on Key Aerodynamic Technologies, Bremen, Germany, 12^{th} to 14^{th} May 2009.
[32] J.-F. LE ROY and S. MORGAND - *SACCON CFD Static and Dynamic Derivatives Using elsA*. AIAA Applied Aerodynamics Conference, Chicago, 28^{th} June to 1^{st} July 2010.
[33] J. DECOURS - *Numerical Approach of Tilt-Rotors*. 10^{th} Onera - DLR Aerospace Symposium, Berlin, 6^{th} to 8^{th} October 2009.

Acronyms

CFD (Computational Fluid Dynamics)
RANS (Reynolds Averaged Navier-Stokes)
DES (Detached Eddy Simulation)
ZDES (Zonal Detached Eddy Simulation)
LES (Large Eddy Simulation)
DNS (Direct Numerical Simulation)
EARSM (Explicit Algebraic Reynolds Stress Model)
DRSM (Differential Reynolds Stress Model)
CAE (Computational AeroElasticity)
MDO (Multi-disciplinary Design Optimization)
UCAV (Unmanned Combat Air Vehicle)
LDV (Laser Doppler Velocimetry)
PIV (Particle Image Velocimetry)
PSP (Pressure Sensitive Paint)
TSP (Temperature Sensitive Paint)
FM (Figure of Merit)
VG (Vortex Generator)
AJVG (Air Jet Vortex Generator)

AUTHORS

Joël Reneaux graduated from the "Arts et Métiers" Engineering school in 1980. At Onera, he has been involved in numerical optimization method applications, helicopter airfoil design, aircraft wing design and laminar flow technology. He is currently Head of the Civil transport Aircraft Unit of the Applied Aerodynamics Department of the Onera Meudon center.

Philippe Beaumier graduated from the "Ecole Centrale de Paris" engineering school in 1989. Since that time, he has been working at Onera in the field of helicopters, with the main emphasis on fluid-structure coupling on main rotor blades, aerodynamic performance prediction and aero-acoustics (BVI noise). He is currently Head of the "Helicopter, Propeller and Turbomachinery" Unit of the Applied Aerodynamics Department of the Onera Meudon center.

Philippe Girodroux-Lavigne engineer who graduated from the "Ecole Centrale de Lyon", has been working at Onera since 1979, first in the "CFD and Aero-acoustics" department, then in the "Aeroelastics and Structural Dynamics" department, where he is involved in numerical aeroelasticity studies for static and dynamic aircraft applications.